Semi-analytical analysis of ground vibration generated at a railway turnout

Pooja Karthik

Witteveen Bos

TU Delft

Semi-analytical analysis of ground vibration generated at a railway turnout

A thesis submitted to the Delft University of Technology in partial fulfillment of the requirements for the degree of

Master of Science in Structural Engineering

by

Pooja Karthik

November 2020

Chairman :	Dr. Ir. K N Van Dalen
TU Delft Supervisor:	Prof. Andrei Metrikine
TU Delft Supervisor:	Ir. Timo Molenkamp
Witteveen + Bos Supervisor:	Dr. Ir. Marieke Bezemer
Witteveen + Bos Supervisor:	Ir. Floris Besseling

ABSTRACT

A railway turnout, which is a combination of a switch and a crossing is an important component in the railway network to divert trains. Due to the change in contact between the wheels and the rails as the train negotiates a turnout, severe impact loading occurs in two-directions: vertically and laterally. These cause negative environmental impacts in terms of ground vibrations. Therefore, understanding the ground response due to a railway turnout qualitatively and quantitatively is essential for soil surface in vicinity.

This thesis focuses on qualitatively and quantitatively describing the ground response through a dual load model setup through semi-analytical approach. A two-dimensional load on a Euler Bernoulli beam which is placed on a three-dimensional half-space is considered to describe the ground response. Followed by which, a load spectrum defining the interaction between the wheels and the rails is considered and the ground response is analysed. Measurements from the vicinity of a turnout is also analysed in order to compare the performance of the model to that of the real-life scenario.

It is further concluded that qualitatively the ground response caused due to impact like loading that occurs at a crossing, and the presence of lateral loading is able to be explained by the model. Quantitatively, to analyse the response recommendations are to be followed to acquire the accurate load spectrum along with considering the complex track geometry for the lateral loading.

Chapter 1 introduces the background of the thesis along with the research objectives and methodology followed.

Chapter 2 studies through literature the cause of impact like loading in a turnout and multiple ways to model them and consequently influencing the modelling choices considered in the following chapters.

Chapter 3 and Chapter 4 proceeds to model an impulse point load on a euler bernoulli beam which is on the surface of a half-space. On modelling, the ground response at points of interest are analysed.

Chapter 5 models a moving load spectrum from the models derived in previous chapters through convolution of responses from moving impulses. The total ground response is then calculated as a super position of responses from the two models derived.

Chapter 6 explains the measurement setup and the ground response from measurements obtained. Further which, the model is updated to meet the standards of the measurements and a comparison is drawn between them.

Chapter 7 lastly concludes the thesis along with suggesting few recommendations and discussing major points of interest.

ACKNOWLEDGEMENTS

This thesis is written in order to obtain the degree of Master of Science in Civil Engineering from Delft University ofTechnology. The research is carried out in collaboration with Witteveen+Bos and the Faculty of Civil Engineering.

I would like to express my sincere gratitude towards my committee members: Dr.Ir. Karel Van Dalen, Ir. Timo Molenkamp and Prof. Andrei Metrikine from TU-Delft and Dr.Ir.Marieke Bezemer and Ir. Floris Besseling from Witteveen+Bos. Thank you to my committee for taking their time in guiding me through my thesis constantly even during the difficult situation of COVID. Through their continual support, interest and guidance from you, I have been able to successfully complete my thesis. I would like to specially thank them for being extremely considerate of my visa extension shortcomings. I would also like to specially thank my daily supervisors: Timo Molenkamp and Marieke Bezemer. Timo's thoughtful understanding and interest in my thesis has led me to perform better, along with his patient explanations to all my doubts, however small they may be. I would like to also thank him for taking his time to read my report and give constructive feedback even at the wake of becoming a new father. Marieke Bezemer has been a constant support through my thesis and she has constantly led me to think outside the box. I would like to thank her for her interest in my thesis and support during the process of taking measurements and analysing them, (right before her holidays) which has helped me beyond measure in completing my thesis on time.

The past two years as a Masters student at TU Delft has aided and polished me further as a Structural Engineer and I thank the faculty of Civil Engineering for it. Most importantly, I am extremely thankful to my parents, Amma and Appa, whose constant support and motivation has got me here and would lead me beyond. Thank You for always seeing the best in me. Thank you to all my friends and family for supporting me through my thesis and my studies. Thank you to my friends whose support and also (their sense of humour) through the COVID-situation made productivity and concentration on my thesis achievable during times of quarantining.

I would like to thank all, my friends, family, committee members without whom I could not have achieved this.

Thank You
Pooja Karthik
20^{th} November 2020

...

CONTENTS

LIST OF FIGURES

LIST OF TABLES

1 INTRODUCTION

1.1 BACKGROUND

Railway switches and crossings are essential in diverting the direction of the train or to cross other tracks. As the railway is a guided way; switches crossings are vital in the working of the railway network. In [Fig.1.1] a standard turnout is depicted which is one of the most commonly used types of switch and crossing combination. It consists of a switch, closure and a crossing panel.

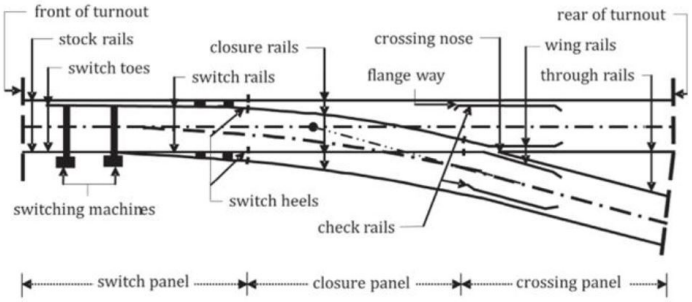

Figure 1.1: Composition of a railway turnout as expressed by Torstensson et al. [2019]

With the increasing population in urban nodes, space constraints lead to densely populated railway-track turnout systems and construction of buildings near them. This poses a problem with regards to ground borne vibrations because railway turnouts are a form of defect-wheel interface Kouroussis et al. [2015a] which causes large impact forces that can propagate to the buildings near-by and cause disturbances Connolly et al. [2016]. Large disturbances occur when the wheels move from stock rail to switch rail in the switch panel and in the crossing panel when the wheels pass the discontinuity between wing and nose rail. These are the source of large dynamic forces, which cause significant ground vibrations in the vicinity of the turnout.
Kouroussis et al. [2015b] highlights in [Fig.1.2] the case of significant difference in levels of vibrations observed between the two cases (standard railway track and in the presence of a defect-switch, crossing etc.), thus showing the significant contribution of local irregularities to vibration levels.

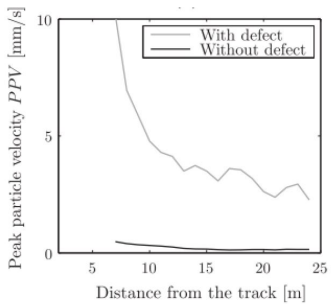

Figure 1.2: Peak particle velocity as a function of the distance from the track related to the passage of an AM96 trainset (2 x 3 carriages) at a speed of 120 km/h as expressed by Kouroussis et al. [2015b]

The lateral vibrations generated in a switch is an important phenomenon to not ignore. In analyzing the effect a turnout has on ground-borne vibrations, lateral source of excitation thus an important aspect as also cited by Burgelman and Bahn [2015]

1.2 PROBLEM DEFINITION

The problem definition encompasses in finding the ground vibrations induced by train-like loading force encountering a railway turnout. The problem is perceived as a three step issue: the vehicle, the track and the soil. The scope of the problem statement revolves around the track system of a turnout and the soil and in particular its effect on the surface vibrations. The vehicle dynamics is out of scope of the problem although the interaction between the vehicle and the tracks is viewed as an application of load.

1.3 OBJECTIVES

The main objective of the thesis is:

"Modelling and analysing the ground vibrations induced by a railway turnout"

The sub-objectives of the thesis are as follows:

1. Modelling and analysing the semi-analytical problem for an impulse point load on a beam interacting with a three dimensional half-space.
2. Modelling and analysing the semi-analytical problem of a moving varying load that represents a turnout force spectrum on a beam interacting with a three dimensional half-space.
3. Validating the model derived ground vibrations to measurements from points near a railway turnout.

1.4 RESEARCH QUESTIONS

The main research question involves :

"Qualitatively and Quantitatively, what are the ground vibrations at points of interest when a train negotiates a railway turnout?"

The sub-research questions are:

1. How to model a semi-analytical model when an impulse point load acts on a beam interacting with a three dimensional half-space and what the conclusions are for the analysis of ground vibrations?
2. How to model a turnout like force spectrum on a 3 dimensional half-space and analyse the ground vibrations caused by it?
3. What conclusions are drawn on comparing the measurements derived ground vibrations to the model considered?

1.5 APPROACH

The approach of the problem statement is a 3 step process as expressed in [Fig.1.3] : Vehicle-Turnout-Soil system.

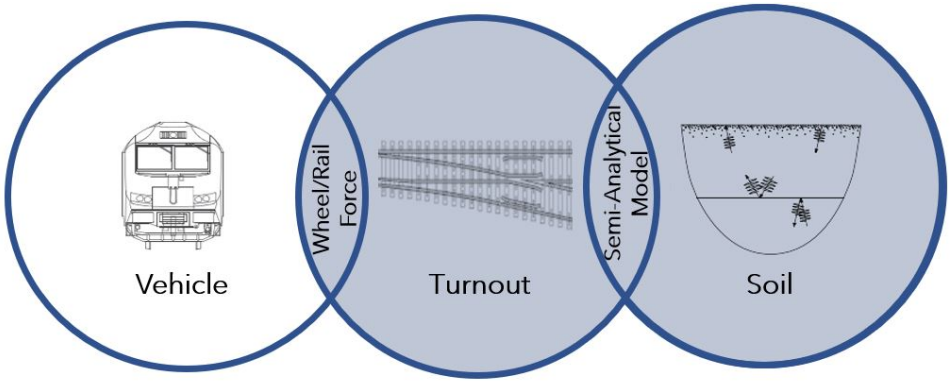

Figure 1.3: 3 system approach highlighting the focused parts

The following explains the 3 system approach:

- **Vehicle** : The vehicle is considered as a combination of point loads on the model. The dynamics and detailing of it is out of scope.
- **Vehicle-Turnout Interaction** : The interaction is in terms of the force spectrum that is input-ed as a load on the turnout. There exists a vertical loading as well as a lateral loading in a turnout. This is considered as two independent problems, which are superimposed.
- **Turnout** : The track system is considered as a Euler-Bernoulli beam.
- **Turnout-Soil Interaction** : The interaction is observed through the concept of equivalent stiffness of the soil provided to the beam when a load is applied on it, as detailed in Dieterman and Metrikine [1996].
- **Soil** : The soil is a three dimensional homogeneous elastic half-space. It is modelled differently for the case of a vertical loading and a lateral loading depending on the decomposition of wave scalar potentials instigated by the loading.

1.5.1 Methodology

The methodology of approach to the problem statement is done in the following steps:

1. Finding the ground response to an impulse point loading in the vertical and lateral direction individually, applied on a beam interacting with a three dimensional half-space.
2. Super-imposing the impulses to form a moving load vertically and laterally that represents a turnout and analysing the ground response.
3. Comparing the built-up model with measurements and analysing the the ground vibrations derived from the two.

2 LITERATURE STUDY

The literature study for the problem statement is approached in the following steps:

1. **Turnout**: Understanding what a turnout is and how & why it is a source of negative effect on ground borne vibrations.
2. **Ground vibration modelling**: Understanding how to model the problem and approach it, therefore defining the consequences of model choices made.
3. **Soil Modelling**: On studying the models, an analytical approach to soil modelling is preferred. Therefore, understanding the soil dynamics is part of the literature study.
4. **Modelling choices**: Certain aspects of the modelling choices made, like the interaction force between the track and soil and the approach to the loading mechanism analogous to vehicle loading is studied.

2.1 TURNOUT

A railway turnout is an important structure in the railway network that let the trains to divert direction [Fig.2.1].As explained by Liu and Markine [2020], a railway turnout has three panels of interest: switch, closure and the crossing panel. The train can move through the direct/main line or towards the branch/ divergent line or route. The switch panel has the switch blades that initiates the diverging direction in the wheels of the trains. In the crossing, which is the point of intersection between the wing rails and the crossing nose (also known as a frog), is a point of gap/ discontinuity that exists when the train finally diverts its direction to the new track line. This discontinuity is a source of high wheel-rail impact Xin et al. [2016], where the wheel forces are two to four times higher than normal track Pletz et al. [2012]. Due to the small curve radii present in the closure panel, lateral wheel forces arise as explained by Burgelman and Bahn [2015] and in the presence of trains consisting of a number of bogies that is pushed through a turnout, the couplers transfer lateral forces rises between them. Due to the complex structure of the turnout system along with impact loading that occurs, they are a source of ground vibrations causing disturbance in neighbouring environment situated near the turnout.

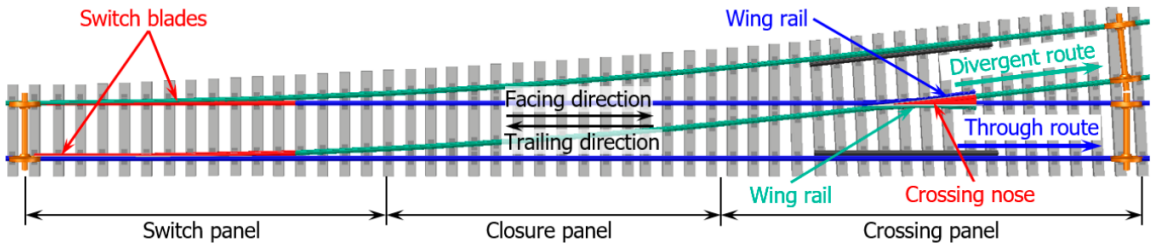

Figure 2.1: Standard railway turnout Liu and Markine [2020]

2.1.1 Source of loading

A railway turnout's complex structure and the change in contact forces is the source of impact loading that occurs in the railway lines. In Alfi and Bruni [2009] a detailed structure of the process of a train moving in a turnout and sequence of contact shifts is explained by [Fig.2.2] and [Fig.2.3] when the wheels negotiate the branch line. In [Fig.2.2] a standard railway turnout is depicted along with notations

on the type of contact between the left wheels and rails in the branch line. By referring to [Fig.2.3], depict the geometry of the wheel-rail contact: the wheel is the flange like structure and the rails are the bottom structure. The contact movement is explained by the grey arrows which denotes contact 1 existing when the train moves on the rails normally, thus generating vertical contact forces. On encountering the switch, the train wheels move gradually to the stock rails, thus generating normal forces at an angle: vertical and lateral forces. The gap or discontinuity in rails at the crossing is represented in the contact 3bl and 4. On passing the turnout, the contact goes back to vertical forces in contact 5.

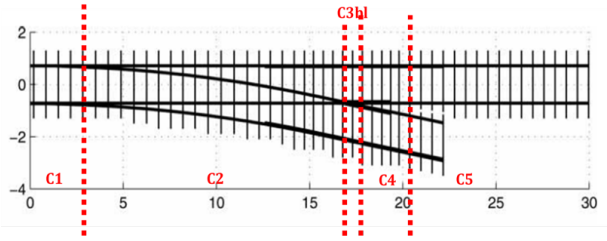

Figure 2.2: Turnout Contact scheme Alfi and Bruni [2009]

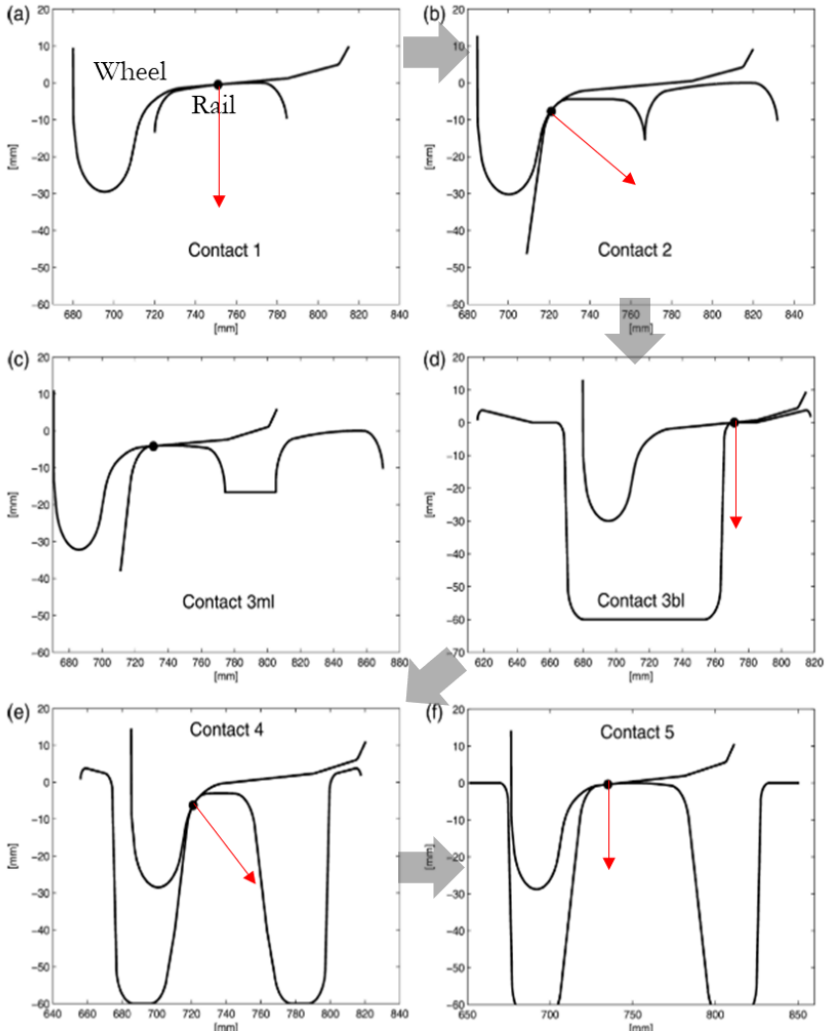

Figure 2.3: Contact scheme Alfi and Bruni [2009]

2.1.2 Loads in a turnout

In Alfi and Bruni [2009] the forces generated in a turnout is mathematically modelled through non hertzian contact modelling and validated against measurements. The model based loads derived when a wheel moves through the branch line at 20 kmph is depicted in [Fig.2.4].The vertical forces generated are almost a constant value of axle loading , and a singular impact like loading at the frog is encountered due to the discontinuity in contact. The lateral forces are generated in the closure panel followed by a singular impact at the crossing.

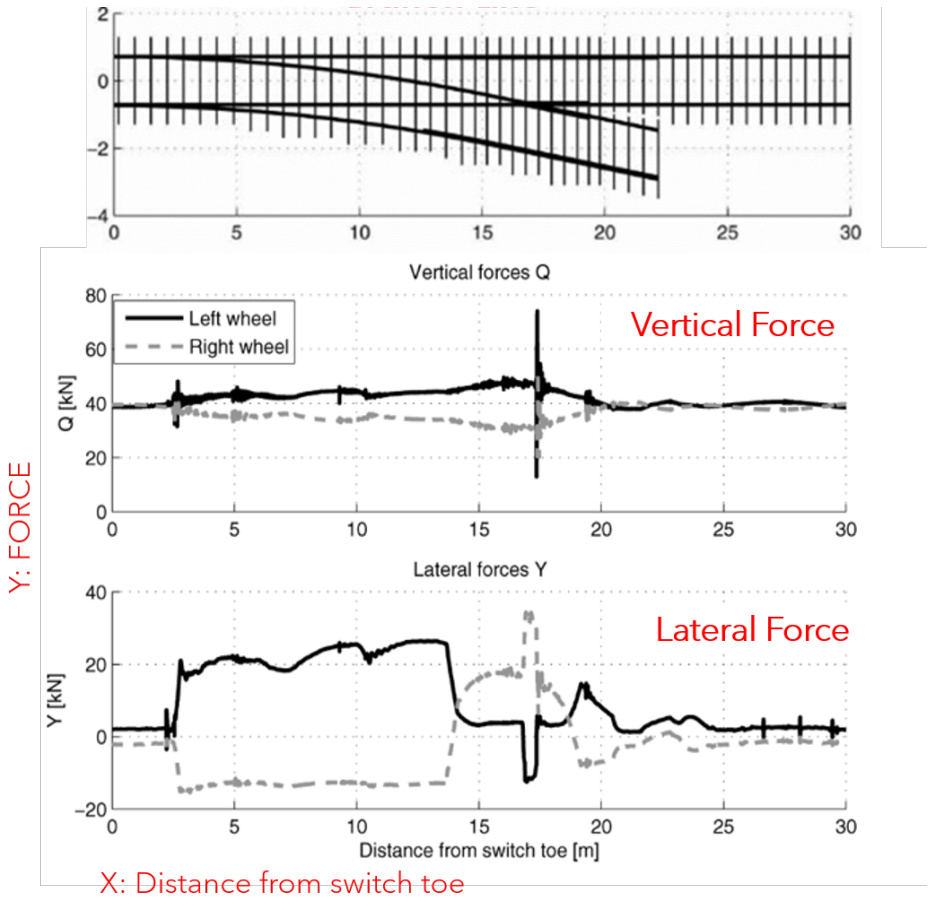

Figure 2.4: Forces in a turnout when the wheels negotiate a branch line at 20 kmph Alfi and Bruni [2009]

2.1.3 Turnout modelling

In Kouroussis et al. [2015b] the environmental effects of ground-borne vibrations due to localised railway defects is analysed. A turnout is modelled as points of singular impact due to the type of loading that occurs [Fig.2.5].In [Fig.2.6] , a crossing is modelled as a sequence of step-up and step-down stepwise contact model where the forces are modelled through non-hertzian contact modelling.

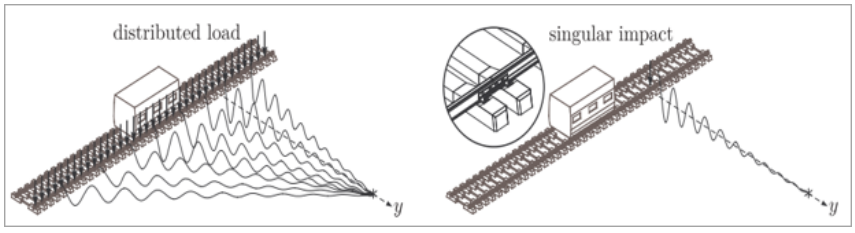

Figure 2.5: Singular impact modelling in Kouroussis et al. [2015b]

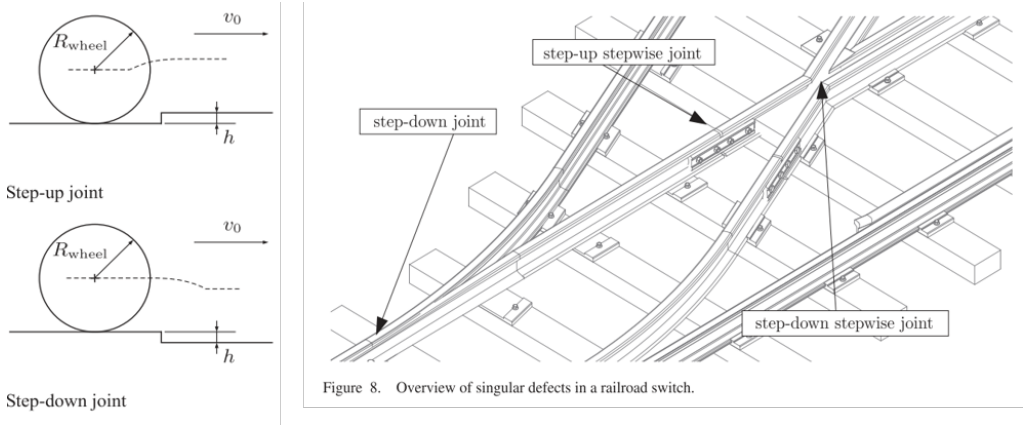

Figure 2.6: Step-up and Step-down model Kouroussis et al. [2015b]

2.2 GROUND VIBRATIONS MODELLING

The approach to the modelling of a ground vibration induced by railway track has been tackled by Kouroussis et al. [2015a] in a three-step approach, which is also applied to the present turnout problem in the following chapters. In [Fig.2.7], the vehicle, track and soil are handled as independent domain problems which are then linked through an interaction model.

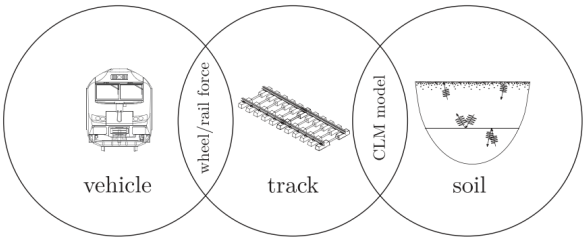

Figure 2.7: Three-step approach model layout by Kouroussis et al. [2015a]

In Connolly et al. [2019], the multiple types of modelling: the vehicle-track and implementation on soil models has been analysed as summarised by [Fig.2.8].

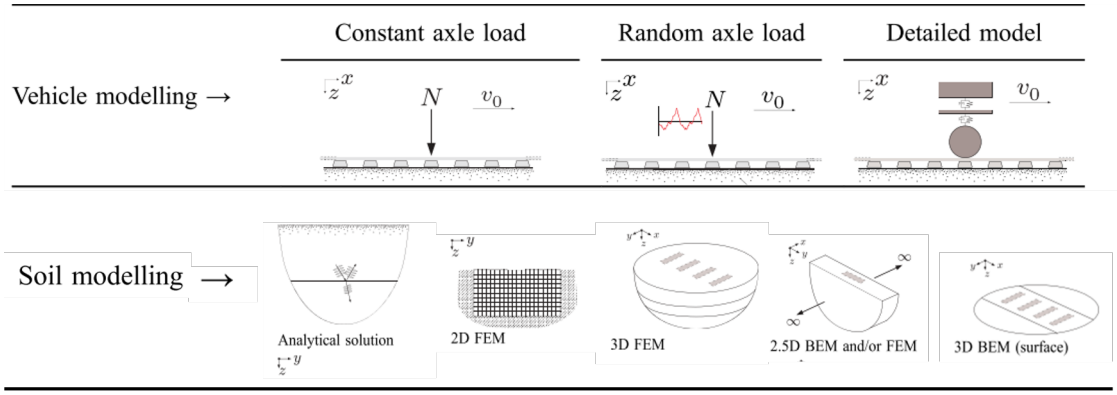

Figure 2.8: Classification of recent railway-induced ground vibration models Connolly et al. [2019]

With reference to the models studied above, the model approached in this thesis is a analytical model of a half-space for the soil with a Euler Bernoulli beam on the surface which has a moving axle load whose magnitude changes with respect to space.

2.3 SOIL MODELLING

2.3.1 Equation of motion

The Caushy-Navier equation or wave equation is one of the basic equations of elastodynamics with reference to J. D. ACHENBACH [2003] expressed as:

$$(\lambda + \mu)\nabla(\nabla \cdot \vec{u}) + \mu\nabla^2\vec{u} + \vec{b} = \rho\ddot{\vec{u}} \tag{2.1}$$

Where the $\vec{u}$ is the displacement vector and $\vec{b}$ is the body force. μ and λ are Lame constants and can be expressed in terms of Young's modulus of the soil (E) and Poisson's ration (ν) as:

$$\lambda = \frac{\nu E}{(1+\nu)(1-2\nu)} \tag{2.2}$$

$$\mu = \frac{E}{2(1+\nu)} \tag{2.3}$$

As any vector can be decomposed into a dot product of a scalar superimposed with a cross product of a vector, the equation of motion of half-space too can be categorised into two types of motion described by Helmholtz wave potentials as:

$$\vec{u} = \nabla\phi + \nabla \times \vec{\psi} \tag{2.4}$$

Where ϕ and ψ refer to two wave scalar potentials which correspond to P and S waves, that is, compression and transverse waves respectively. Therefore, the wave potentials can be decomposed into two equations as:

$$\ddot{\phi} = \alpha^2\nabla^2\phi \tag{2.5}$$

$$\ddot{\vec{\psi}} = \beta^2\nabla^2\vec{\psi} \tag{2.6}$$

Where $\alpha, \beta = c_{l,t}$ which refer to the speed of compression and transverse waves as described as:

$$c_l = \sqrt{\frac{\lambda + 2\mu}{rho}} \tag{2.7}$$

$$c_t = \sqrt{\frac{\mu}{\rho}} \tag{2.8}$$

2.3.2 Lamb's wave potentials

From Aki and G.Richards [2002], for a medium where material discontinuities exist horizontally like a half-space, P and SV plane waves are coupled whereas SH waves propagate independently. Therefore, from Lame's theorem, the wave potentials can be described as:[Eq.2.9-2.10], where $\alpha, \beta = c_{l,t}$ and $c_{l,t}$ refers to the speed of longitudinal and transverse waves in the medium.

$$\ddot{\phi} = \alpha^2\nabla^2\phi \tag{2.9}$$

$$\ddot{\vec{\psi}} = \beta^2\nabla^2\vec{\psi} \tag{2.10}$$

There the displacement vector can be expressed in terms of wave potential as[Eq.2.11]:

$$\vec{u} = \nabla\phi + \nabla \times \vec{\psi} \tag{2.11}$$

Where the following conditions are met [Eq.2.12-2.13]:

$$\nabla.\vec{\psi} = 0 \tag{2.12}$$

$$\nabla.\phi = 0 \tag{2.13}$$

In the absence of any body forces, the displacement is a decomposed into three scalar equations as [Eq.2.14-2.16]:

$$\ddot{\phi} = \alpha^2 \phi \tag{2.14}$$

$$\frac{\partial^2}{\partial t^2}(\nabla \times \vec{\psi})_z = \beta^2 \nabla^2 [(\nabla \times \vec{\psi})_z] \tag{2.15}$$

$$\ddot{\psi}_z = \beta^2 \nabla^2 \psi_z \tag{2.16}$$

When no body forces exist, any motion can be decomposed into three kinds of motion as when two out of three functions vanish everywhere: ϕ, $(\nabla \times \vec{\psi})_z$, ψ_z:

- Firstly, when $(\nabla \times \vec{\psi})_z$, ψ_z are zero everywhere. This is when there are P-waves. They are defined by nonzero $\nabla.\vec{u}$, but $\nabla \times \vec{u} = 0$
- Secondly, when $\phi = 0$ and $\psi_z = 0$. As by definition $\nabla.\psi = 0$, it is derived that $\frac{\partial \psi_x}{\partial x} + \frac{\partial \psi_y}{\partial y} = 0$. This concludes that there exists there exists a function M such that $\psi_x = \frac{\partial M}{\partial y}$, $\psi_y = -\frac{\partial M}{\partial x}$, that is $\vec{\psi} = \nabla \times (0, 0, M)$, On rewriting M as a scalar function called ψ, $\vec{u}$ is re-written as [Eq.2.17]:

  $$\vec{u} = \nabla \times \nabla \times (0, 0, \psi) = (\frac{\partial^2 \psi}{\partial z \partial x}, \frac{\partial^2 \psi}{\partial z \partial y}, -\frac{\partial^2 \psi}{\partial x^2} - -\frac{\partial^2 \psi}{\partial y^2}) \tag{2.17}$$

  SV waves fall into this kind of motion as $\nabla.\vec{u} = 0$ and $(\nabla \times \vec{u})_z = 0$.
- Thirdly, when $\phi = 0$ and $(\nabla \times \vec{u})_z = 0$, then $\nabla.\vec{u} = 0$ and $u_z = 0$. Therefore there exists a function ψ such that $\vec{u} = \nabla \times (0, 0, \chi)$. This is the SH wave motion.

Therefore, as $\vec{u}$ can be split into three kinds of motion: P, SV and SH waves and can be expressed as[Eq.2.18]:

$$\vec{u} = \nabla\phi + \nabla \times \nabla \times (0, 0, \psi) + \nabla \times (0, 0, \chi) \tag{2.18}$$

Where the three wave scalar potentials are expressed by [Eq.2.19-2.21]

$$\ddot{\phi} = \alpha^2 \nabla^2 \phi \tag{2.19}$$

$$\ddot{\psi} = \beta^2 \nabla^2 \psi \tag{2.20}$$

$$\ddot{\chi} = \beta^2 \nabla^2 \chi \tag{2.21}$$

2.4 MODELLING CHOICES

2.4.1 Interaction: Equivalent Stiffness

In Dieterman and Metrikine [1996] a half-space is considered where a Euler Bernoulli beam of width $2a$ is present on the surface [Fig. 2.9]. The beam and soil are decoupled domains in which the soil is perceived as frequency dependent springs for the beam domain and the beam is perceived as an external load in the soil domain. The concept of equivalent stiffness and the process of solving it in the wavenumber-frequency domain is followed in the coming chapters.

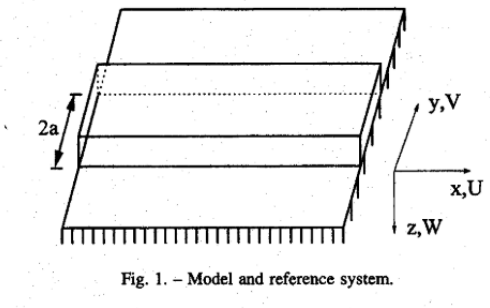

Fig. 1. – Model and reference system.

Figure 2.9: Model Dieterman and Metrikine [1996]

2.4.2 Loading method

In Sheng [1999], dynamic response of a half-space to a harmonic load moving along the rails has been discussed. The dynamic loads, moving constant axle loads and moving dynamic loads can be used in the model proposed in the paper. The concept of application of a moving impulse load in Chapter 5 has been derived from the mentioned paper. Perceiving the load from a frequency domain point of view, the the harmonic load considered in Sheng [1999] has a magnitude of P_o at only a single frequency (ω_o), whereas in Chapter 5, the load is considered to be an impulse which is moving, it has a magnitude of P_o at all frequencies.

3 VERTICAL IMPULSE

The chapter comprises the analytical solution of ground vibrations due to a vertical point impulse load acting on the beam that is supported by an elastic half-space. The interacting forces between beam and half-space are obtained by making use of the equivalent stiffness of the soil. The first system that is solved is an infinite Euler-Bernoulli beam in interaction with frequency-dependent springs, representing the soil. Hereafter the spring forces are taken as excitation force on the soil, spread over the width of the beam. The problem is solved in the frequency domain and the results are analysed in the time domain.

3.1 MODEL

The model consists of 2 linear subdomains: Ω_b and Ω_s which refers to the beam and the half-space respectively.[Fig.3.1]

- **Beam(Ω_b)** : A Euler Bernoulli beam of width $2a$ (y-direction) and of infinite length (x-direction) is present on a 3 dimensional half-space(x, y, z). The beam's flexural rigidity (EI) and mass per unit length (m) are assumed to be longitudinally invariant.
- **Half-space(Ω_s)**: The half-space is an elastic, homogeneous and isotropic medium defined by Lamb's equations. (Lamb [1904])
- **Force**: An impulse at t=0 is applied at the origin (0,0) ,on the beam along the z-direction (referred to as vertical)
- **Interaction**: The interaction between the two domains (Ω_b, Ω_s) is achieved through enforcing displacement continuity about the mid-line of the beam and stress continuity over the width of the beam (2a). The linear approach leads to the concept of equivalent stiffness which is the key interaction factor as derived in Dieterman and Metrikine [1996]. It is dependent on the frequency, spatial coordinate along length (x-direction) and displacement of the beam at the coordinate. The interaction force that is caused due to the loading on the beam which is resisted by the soil through this force, is in turn the loading force on the soil. Therefore, this is the direct cause of excitation of ground vibrations in the soil.

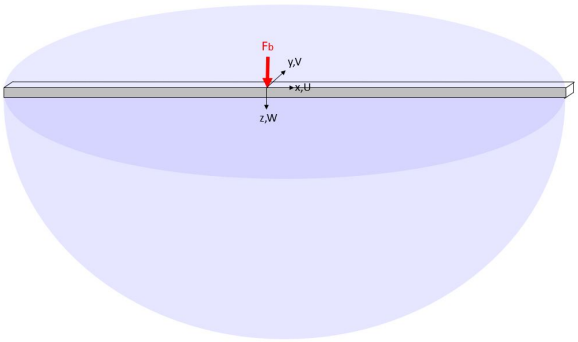

Figure 3.1: Representation of Model-1

3.2 GOVERNING EQUATIONS: SPACE-TIME

Half-space

The equation of motion of half-space (Ω_s) is [Eq.3.1]:

$$\mu\nabla^2\vec{u} + (\lambda+\mu)\nabla\nabla\cdot\vec{u} = \rho\frac{\partial^2\vec{u}}{\partial t^2} \tag{3.1}$$

$\vec{u}$ is the displacement vector of half-space in x, y and z respectively [Eq. 3.2.], μ is the shear modulus and λ is Lame's constant.

$$\vec{u}(x,y,z,t) = \{U(x,y,z,t), V(x,y,z,t), W(x,y,z,t)\} \tag{3.2}$$

In coordination with scalar potentials derived in Lamb [1904] the displacements are expressed as [Eq. 3.3-3.5]:

$$U = \frac{\partial\phi}{\partial x} + \frac{\partial^2\psi}{\partial x\partial z} \tag{3.3}$$

$$V = \frac{\partial\phi}{\partial y} + \frac{\partial^2\psi}{\partial y\partial z} \tag{3.4}$$

$$W = \frac{\partial\phi}{\partial z} + \frac{\partial^2\psi}{\partial z^2} - \frac{1}{c_{t^2}}\frac{\partial^2\psi}{\partial t^2} \tag{3.5}$$

The equation of motion of half-space [Eq.3.1] in terms of scalar potential is [Eq.3.6-3.7].

$$\nabla^2\phi = \frac{1}{c_l^2}\frac{\partial^2\phi}{\partial t^2} \tag{3.6}$$

$$\nabla^2\psi = \frac{1}{c_t^2}\frac{\partial^2\psi}{\partial t^2} \tag{3.7}$$

c_l and c_t are the speed of the longitudinal and transverse waves in the half-space, respectively.

Beam

The equation of motion of the beam is [Eq. 3.8]:

$$m\frac{\partial^2 W^o}{\partial t^2} + EI\frac{\partial^4 W^o}{\partial x^4} = F_s(x,t,W^o(x,t)) + F_b(x,t) \tag{3.8}$$

W^o is the displacement of the beam in the z direction, F_s is the interacting force between the beam and the soil and F_b is the force exerted on the beam by an external source. An important property to note is the nature of these forces; F_b and F_s acts on an Euler Bernoulli beam, due to its spatial one dimensional nature, it is a force that is only dependent on x-direction (along length of the beam) and time.

Boundary Conditions

The boundary conditions of the half-space are [Eq. 3.9-3.11]:

$$2a\sigma_{zz}(x,y,0,t) = F_s(x,t,W^o(x,t)(H(y+a) - H(y-a)) \tag{3.9}$$

$$\tau_{xz}(x,y,0,t) = 0 \tag{3.10}$$

$$\tau_{yz}(x,y,0,t) = 0 \tag{3.11}$$

Interface condition between the domains Ω_b and Ω_s:

$$W(x,0,0,t) = W^o(x,t) \tag{3.12}$$

An interesting perspective is in exertion of the interaction force, F_s. It is lumped to one dimension on the beam but when exerted on the half-space it is evenly spread over the width 2a of the beam

Space-Time	Wavenumber-Frequency
$\phi(x,y,z,t)$	$f(k_1,k_2,z,\omega)$
$\psi(x,y,z,t)$	$g(k_1,k_2,z,\omega)$
$W^o(x,t)$	$h(k_1,\omega)$
$F_b(x,t)$	$\tilde{f}_b(k_1,\omega)$
$F_s(x,t,W^0(x,t))$	$\tilde{f}_s(k_1,\omega,h(k_1,\omega))$

Table 3.1: Fourier Transform notation

(2-dimensional). Consequently, the robustness of this assumption is acceptable under the clause that the waves in beams have a wavelength much higher than the width of the beam. The simplistic duality in the application of F_s, is referred from Dieterman and Metrikine [1996] aids in further sections. For low frequency content, the above boundary condition suffices as concluded in Steenbergen and Metrikine [2007].
The stresses in terms of wave potential are expressed as [Eq.3.13-3.15]:

$$\sigma_{zz} = \frac{\lambda}{c_l^2}\frac{\partial^2\phi}{\partial t^2} + 2\mu\left(\frac{\partial^2\phi}{\partial z^2} + \frac{\partial^3\psi}{\partial z^3}\right) - 2\rho\frac{\partial^3\psi}{\partial z\partial t^2} \tag{3.13}$$

$$\tau_{xz} = 2\mu\left(\frac{\partial^2\phi}{\partial x\partial z} + \frac{\partial^3\psi}{\partial x\partial z^2}\right) - \rho\frac{\partial^3\psi}{\partial x\partial t^2} \tag{3.14}$$

$$\tau_{yz} = 2\mu\left(\frac{\partial^2\phi}{\partial y\partial z} + \frac{\partial^3\psi}{\partial y\partial z^2}\right) - \rho\frac{\partial^3\psi}{\partial y\partial t^2} \tag{3.15}$$

3.3 GOVERNING EQUATIONS – WAVENUMBER–FREQUENCY DOMAIN

3.3.1 Forward Fourier Transform

The governing equations of motion described in section 3.2 is transformed to wavenumber-frequency domain as [Eq.3.16], where F is any function in wavenumber-frequency domain and f is the fourier image of F in the space-time domain :

$$F(k_1,k_2,z,\omega) = \int_{-\infty}^{\infty}\int_{-\infty}^{\infty}\int_{-\infty}^{\infty} f(x,y,z,t)e^{i(\omega t - k_1 x - k_2 y)}dtdxdy \tag{3.16}$$

On fourier transforming the governing equations, the notations of relevant terms are expressed in Table:3.1.

3.3.2 Governing equations

The equations of motion of the half-space are [Eq.3.17-3.18], where f and g are the wavenumber-frequency domain Fourier images of the wave scalar potentials ϕ, ψ:

$$\frac{\partial^2 f(k_1,k_2,z,\omega)}{\partial z^2} + \left(\frac{\omega^2}{c_l^2} - k_1^2 - k_2^2\right)f(k_1,k_2,z,\omega) = 0 \tag{3.17}$$

$$\frac{\partial^2 g(k_1,k_2,z,\omega)}{\partial z^2} + \left(\frac{\omega^2}{c_t^2} - k_1^2 - k_2^2\right)g(k_1,k_2,z,\omega) = 0 \tag{3.18}$$

The equation of motion of the beam is:

$$h(\omega,k_1)D(\omega,k_2) = \tilde{f}_s(\omega,k_1,h(\omega,k_1)) + \tilde{f}_b(\omega,k_1) \tag{3.19}$$

Where the dispersion equation of the beam, $D(\omega, k_1) = -m\omega^2 + EIk_1^4$
The boundary conditions of half-space is [Eq.3.20-3.21]:

$$\frac{-\omega^2\lambda}{c_l^2}f + 2\mu(\frac{\partial^2 f}{\partial z^2} + \frac{\partial^3 g}{\partial z^3}) + 2\rho\omega^2\frac{\partial g}{\partial z} = \tilde{f}_s\frac{sin(ak_2)}{ak_2} \tag{3.20}$$

$$2\mu(\frac{\partial^2 f}{\partial z^2} + \frac{\partial^2 g}{\partial z^2}) + \rho\omega^2 g = 0 \tag{3.21}$$

The interface condition is [Eq.3.22]:

$$h(\omega, k_1) = \frac{1}{2\pi}\int_{-\infty}^{\infty} w(k_1, k_2, 0, \omega)dk_2 \tag{3.22}$$

Where $w(k_1, k_2, z, \omega) = \int_{-\infty}^{\infty}\int_{-\infty}^{\infty}\int_{-\infty}^{\infty} W(x, y, z, t)e^{i(\omega t - k_1 x - k_2 y)}dtdxdy$ which is the fourier transform of the half-space displacement W. On convolution along k_2, the interface condition of the condition of equal displacements about the mid-line of the beam is linked to that of the half-space.

3.4 SOLUTION TO GOVERNING EQUATIONS

Owing to the characteristics of a half-space the equation of motion corroborating with Sommerfield's radiation condition is [Eq. 3.23-3.24]:

$$f(k_1, k_2, z, \omega) = A(k_1, k_2, \omega)e^{-zR_l} \tag{3.23}$$

$$g(k_1, k_2, z, \omega) = B(k_1, k_2, \omega)e^{-zR_t} \tag{3.24}$$

Where A,B are viewed as horizontal wave functions as described by Aki and G.Richards [2002] as they hold the information of the wave potential along k_1, k_2 and does not depend on z direction.The exponent term is the function that prescribes the wave potential's value along z, therefore $R_{l,t}$ is [Eq.3.25] :

$$R_{l,t} = \begin{cases} \sqrt{(k_1^2 + k_2^2) - \frac{\omega^2}{c_{l,t}^2}} & \text{if } \frac{\omega^2}{c_{l,t}^2} < k_1^2 + k_2^2 \\ i\sqrt{\frac{\omega^2}{c_{l,t}^2} - (k_1^2 + k_2^2)} & \text{if } \frac{\omega^2}{c_{l,t}^2} > k_1^2 + k_2^2 \end{cases} \tag{3.25}$$

On substituting the equation of motion of half-space [Eq.3.23-3.24] in the boundary conditions, linear equations obtained are:

$$(\frac{-\omega^2\lambda}{c_l^2} + 2\mu R_l^2)A - 2R_t(\mu R_t^2 + \rho\omega^2)B = \tilde{f}_s(\omega, k_1, h(\omega, k_1))\frac{sin(ak_2)}{ak_2} \tag{3.26}$$

$$(-2\mu R_l)A + (2\mu R_t^2 + \rho\omega^2)B = 0 \tag{3.27}$$

Solving for A and B leads to:

$$A = \tilde{f}_s\frac{2R_t^2 + \frac{\omega^2}{c_t^2}}{\mu\Delta(k_1, k_2, \omega)}\frac{sin(ak_2)}{ak_2} \tag{3.28}$$

$$B = \tilde{f}_s\frac{2R_l}{\mu\Delta(k_1, k_2, \omega)}\frac{sin(ak_2)}{ak_2} \tag{3.29}$$

Where, $\Delta(k_1, k_2, \omega) = (2(k_1^2 + k_2^2) - \frac{\omega^2}{c_t^2})^2 - 4R_l R_t(k_1^2 + k_2^2)$

3.4.1 Equivalent Stiffness

In order to find the interaction force F_s, it is essential to solve for equivalent stiffness of the interaction. Let us assume that no external load acts and proceed by solving the interface condition [Eq.3.22].The fourier image of the half-space displacement along z is [Eq.3.30]

$$w(k_1, k_2, z, \omega) = \frac{\partial f}{\partial z} + \frac{\partial^2 g}{\partial z^2} + \frac{\omega^2}{c_t^2}g \tag{3.30}$$

The beam's equation of motion is now:

$$\tilde{f_s}(\omega, k_1, h(\omega, k_1)) = h(\omega, k_1) D(\omega, k_1) \tag{3.31}$$

On substituting [Eq. 3.23-3.24] in [Eq.3.30] with the derived expressions of A,B, at z=0, and keeping in mind that the interaction force is expressed as [Eq.3.31], the interface condition can then be re-phrased as [Eq.3.32]

$$w(k_1, k_2, 0, \omega) = \frac{\omega^2 R_l}{\mu c_t^2} \frac{h(\omega, k_1) D(\omega, k_1)}{\Delta(\omega, k_1, k_2)} \frac{sin(ak_2}{ak_2} \tag{3.32}$$

Substituting [Eq.3.32] in [Eq.3.22] :

$$h(\omega, k_1) \left\{ 1 - \frac{\omega^2 D(\omega, k_1)}{2\pi\mu c_t^2} \int_{-\infty}^{\infty} \frac{R_l}{\Delta} \frac{sin(ak_2)}{a_k 2} dk_2 \right\} \tag{3.33}$$

[Eq.3.33] can also be viewed as: $h(\omega, k_1) D(\omega, k_1) + \chi(\omega, k_1) = 0$ and with reference to Dieterman and Metrikine [1996] the equivalent stiffness of the half-space is χ from the mentioned form of equation. Therefore:

$$\chi(\omega, k_1) = \frac{-2\pi\mu c_t^2}{\omega^2} \left(\int_{-\infty}^{\infty} \frac{R_l}{\Delta} \frac{sin(ak_2)}{ak_2} dk_2 \right)^{-1} \tag{3.34}$$

Where $\Delta(k_1, k_2, \omega) = (2(k_1^2 + k_2^2) - \frac{\omega^2}{c_t^2})^2 - 4R_l R_t (k_1^2 + k_2^2)$ and $R_{l,t}$ follows the condition in [Eq.3.25].

3.4.2 Interaction force

From the equivalent stiffness derived in [Eq.3.34] for no external loading:

$$\begin{aligned} \tilde{f_s} &= h(\omega, k_1) D(\omega, k_1) \\ \text{Also} &: h(\omega, k_1)(D(\omega, k_1) + \chi(\omega, k_1)) = 0 \\ \text{Therefore} &: \tilde{f_s} = -h(\omega, k_1) \chi(\omega, k_1) \end{aligned} \tag{3.35}$$

Similarly, for the case of external loading, the equations can be re-phrased as:

$$\begin{aligned} h(\omega, k_1)(D(\omega, k_1) + \chi(\omega, k_1)) &= \tilde{f_b}(\omega, k_1) \\ \text{Therefore} &: \tilde{f_s} = -\frac{\tilde{f_b}(\omega, k_1) \chi(\omega, k_1)}{D(\omega, k_1) + \chi(\omega, k_1)} \end{aligned} \tag{3.36}$$

3.5 SURFACE DISPLACEMENT

The displacements of the half-space in the wave-number frequency domain are [Eq.3.37]:

$$\begin{aligned} \tilde{u} &= -ik_1 (f + \frac{\partial g}{\partial z}) \\ \tilde{v} &= -ik_2 (f + \frac{\partial g}{\partial z}) \\ \tilde{w} &= \frac{\partial f}{\partial z} + \frac{\partial^2 g}{\partial z^2} + \frac{\omega^2}{c_t^2} g \end{aligned} \tag{3.37}$$

At z=0 ,the displacements are [Eq.3.38]:

$$\begin{aligned} \tilde{u} &= ik_1 (2R_t^2 + \frac{\omega^2}{c_t^2} - 2R_t R_l) \frac{\tilde{f_s}(k_1, \omega)}{\mu\Delta(k_1, k_2, \omega)} \frac{sin(ak_2)}{ak_2} \\ \tilde{v} &= ik_2 (2R_t^2 + \frac{\omega^2}{c_t^2} - 2R_t R_l) \frac{\tilde{f_s}(k_1, \omega)}{\mu\Delta(k_1, k_2, \omega)} \frac{sin(ak_2)}{ak_2} \\ \tilde{w} &= -\frac{\omega^2}{c_t^2} R_l \frac{\tilde{f_s}(k_1, \omega)}{\mu\Delta(k_1, k_2, \omega)} \frac{sin(ak_2)}{ak_2} \end{aligned} \tag{3.38}$$

Domain (Ω)	Name	Value	Unit
Half-space	Shear Modulus of half-space (μ)	3.27×10^7	N/m^2
	Poisson's Ratio (ν)	0.3	
	Material Damping	2.5 %	
	Density of half-space (ρ)	1960	kg/m^3
	Longitudinal wave speed (c_l)	$242.34 + 6.05i$	m/s
	Transverse wave speed (c_t)	$119.97 + 2.99i$	m/s
	Rayleigh wave speed (c_r)	$129.54 + 3.23i$	m/s
Beam	Mass of beam (m)	760	kg/m
	Flexural Rigidity (EI)	1.29×10^7	Nm^2
	Width of beam (2a)	2×2.6	m
Force	Axle load on beam (F_b)	$225\delta(x)\delta(t)$	kN

Table 3.2: Numerical Model Details

3.5.1 Inverse Fourier Transform

Inverse fourier transform of surface displacements [Eq.3.38] to the frequency domain are [Eq. 3.39]:

$$\begin{aligned}
\tilde{U}(x,y,0,\omega) &= \frac{1}{4\pi^2}\int_{-\infty}^{\infty}\int_{-\infty}^{\infty} ik_1(2R_t^2 + \frac{\omega^2}{c_t^2} - 2R_tR_l)\frac{\tilde{f}_s(k_1,\omega)}{\mu\Delta(k_1,k_2,\omega)}\frac{sin(ak_2)}{ak_2}e^{ik_1x+ik_2y}dk_1dk_2 \\
\tilde{V}(x,y,0,\omega) &= \frac{1}{4\pi^2}\int_{-\infty}^{\infty}\int_{-\infty}^{\infty} ik_2(2R_t^2 + \frac{\omega^2}{c_t^2} - 2R_tR_l)\frac{\tilde{f}_s(k_1,\omega)}{\mu\Delta(k_1,k_2,\omega)}\frac{sin(ak_2)}{ak_2}e^{ik_1x+ik_2y}dk_1dk_2 \\
\tilde{W}(x,y,0,\omega) &= \frac{1}{4\pi^2}\int_{-\infty}^{\infty}\int_{-\infty}^{\infty} -\frac{\omega^2}{c_t^2}R_l\frac{\tilde{f}_s(k_1,\omega)}{\mu\Delta(k_1,k_2,\omega)}\frac{sin(ak_2)}{ak_2}e^{ik_1x+ik_2y}dk_1dk_2
\end{aligned} \tag{3.39}$$

In order to obtain the time domain displacements, the functions are inverse fourier transformed again [Eq. 3.40]

$$\begin{aligned}
U(x,y,0,t) &= \frac{1}{2\pi}\int_{-\infty}^{\infty}\tilde{U}(x,y,0,\omega)e^{-i\omega t}d\omega \\
V(x,y,0,t) &= \frac{1}{2\pi}\int_{-\infty}^{\infty}\tilde{V}(x,y,0,\omega)e^{-i\omega t}d\omega \\
W(x,y,0,t) &= \frac{1}{2\pi}\int_{-\infty}^{\infty}\tilde{W}(x,y,0,\omega)e^{-i\omega t}d\omega
\end{aligned} \tag{3.40}$$

3.5.2 Numerical Solution-MATLAB

The surface displacements are calculated and inverse fourier transformed numerically using MATLAB. Table-3.2 are the model details considered as input with reference to Dieterman and Metrikine [1996]. Damping of 5% is included in the frequency domain and provided via a complex shear modulus of the half-space

3.6 RESULT

For a point load acting as an impulse at the origin on the beam, the points of discussion that is vital for understanding the problem and the solution are:

- The interacting force (F_s) : For an impulse that is applied, F_s is analysed for multiple frequencies, to notice how it behaves in the space domain. This is the loading problem on the half-space. The spatial as well as time smearing nature of the interacting force, is essential in a railway schematic problem.

- The surface displacements (U, V, W) : The displacements in the frequency domain as well as time domain is essential notice as this is the solution.

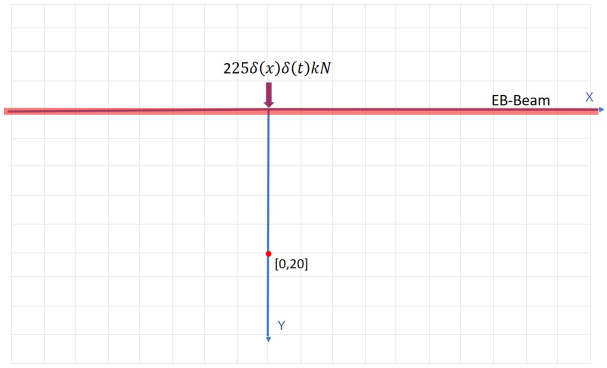

Figure 3.2: Model and Point of interest

3.6.1 Interacting force

The interacting force, [Eq.3.36] is a function of the applied load $(\tilde{f}_b)$, the equivalent stiffness between the domains (χ) and the dispersion equation of the beam (D). Therefore, it is essentially observed in the ω-k_1 domain. For $F_b(x,t)$ being a $225kN\delta(x)\delta(t)$, the Fourier transform of it is $\tilde{f}_b(\omega,k_1) = 225 \times 10^3$. Therefore,

$$\begin{aligned} \tilde{f}_s(\omega,k_1) &= -\frac{225 \times 10^3 \chi(\omega,k_1)}{D(\omega,k_1)+\chi(\omega,k_1)} \\ \chi(\omega,k_1) &= \frac{-2\pi\mu c_t^2}{\omega^2}\left(\int_{-\infty}^{\infty} \frac{R_l}{\Delta}\frac{sin(ak_2)}{ak_2}dk_2\right)^{-1} \\ D(\omega,k_1) &= -m\omega^2 + EIk_1^4 \end{aligned} \tag{3.41}$$

In Fig.3.3 the interaction force as a function of distance is expressed for 5, 25 and 50Hz.

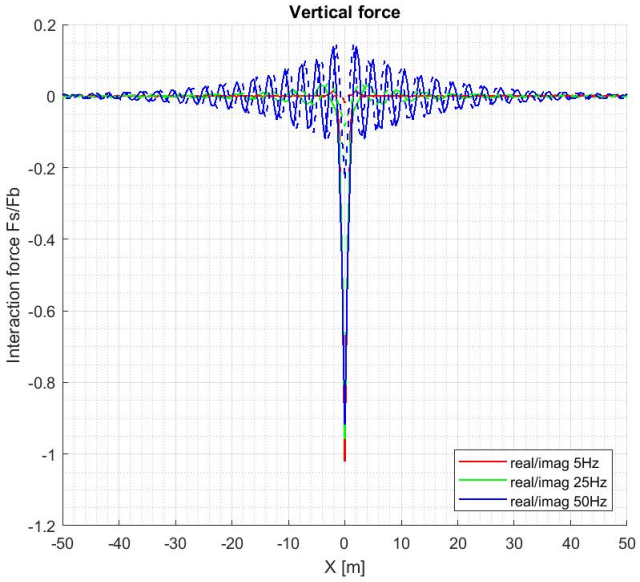

Figure 3.3: Interaction force at 5, 25 and 50 Hz of Loading frequency

3.6.2 Surface displacements

The displacements at $z = 0$ m, is found from the Eq.3.39 on numerically integrating them. Fig.3.4 contains the displacements along y=0, i.e. right under the mid line of the beam. The displacements along y (V) is zero, due to symmetry of the half-space problem. The displacement along x (U) is anti-symmetric in nature at y=0 due to the symmetry of the infinitely long beam.At the point of application of load U=0, due to loading condition being constrained only to z. The displacement along z (W) is comparatively the highest and this is due to the half-space($z > 0$ system) and loading nature. With respect to loading frequencies, it can also be noticed that the wave-numbers increase with higher frequency of loading.

In Fig.3.5 the displacements along y=10, i.e. 10 m away from the beam is derived. The important observation is that U,V and W are present in almost comparative range. U is anti-symmetric about x=0 whereas V and W are symmetric in nature.This is essentially due to the symmetric nature of the system and loading again.

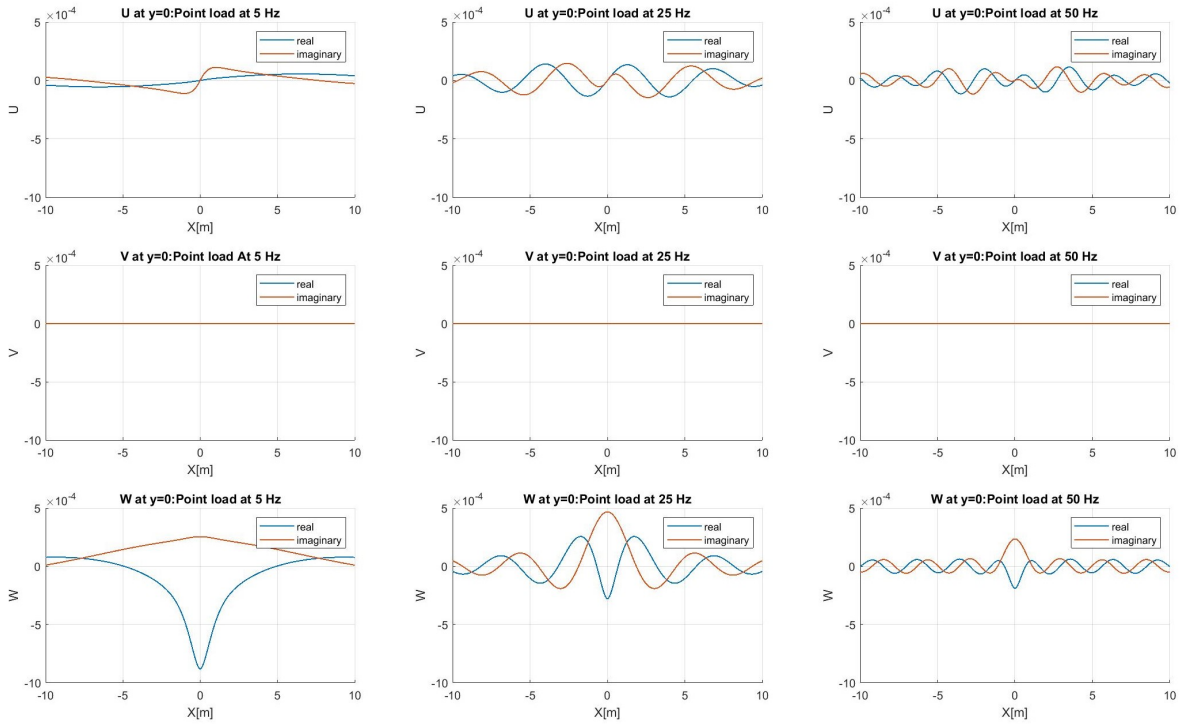

Figure 3.4: Surface displacements at y=0 when loading frequency is 5, 25 and 50 Hz

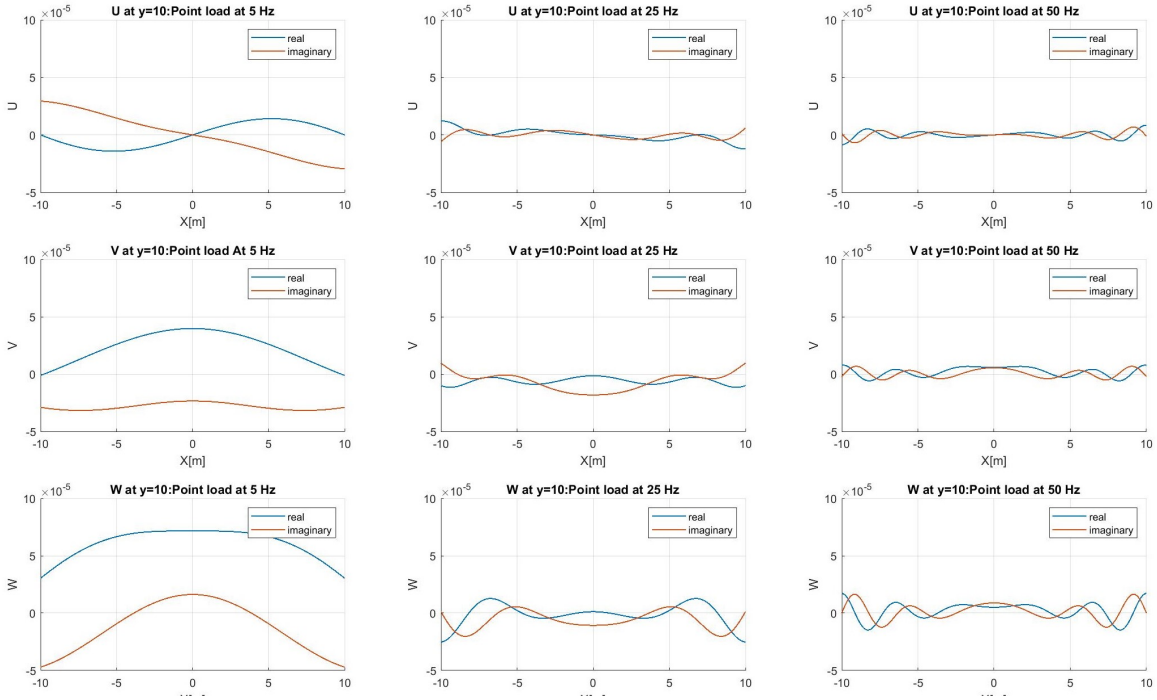

Figure 3.5: Surface displacements at y=10 when loading frequency is 5, 25 and 50 Hz

3.6.3 Point of Interest

For a point of interest, example [0,20] as notated in Fig.3.2 the frequency domain result of the three-dimensional velocities can be found.[Fig.3.6] refers to this, and as expected that U=0 due to symmetry and V, W are in comparison range, with W> V on an average. The disturbance noticed at time $t = 0$ is due to numerical truncation in the frequency domain at $f = 250$ Hz.

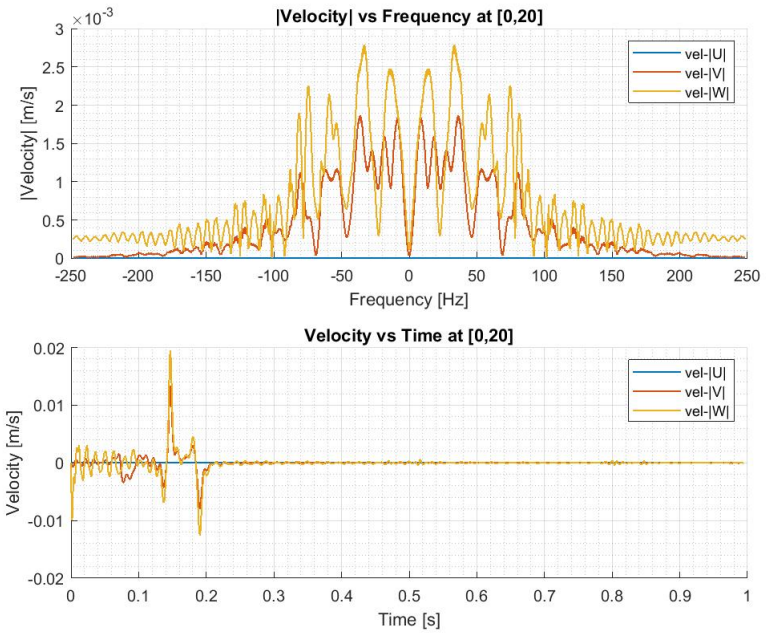

Figure 3.6: Surface velocity [0,20] when an impulse of 225 KN acts at the origin on the beam

3.6.4 Multiple points of interest

Diagonally from the point of loading, four points of interest are considered with radial distances of 10, 20, 30, 40 m on the surface [Fig.3.7]. The displacements at these points are plotted for an impulse point load at the origin on the beam [Fig.3.8]. The arrival of waves is calculated from the speeds in Table:3.3. The points to notice are:

- The attenuation in waves along the distance is observed from the magnitude of displacements, due to geometrical damping.
- U, V are almost equal for higher distances, which can be inferred that at higher distances the beam's influence is reduced. Whereas, at $r = 10$ m, the values of U, V are different.
- The P-wave arrival is significant in U, V when compared to W as they are significant in along the surface direction.
- The time difference between the arrival of P-wave and surface waves is higher for higher distances.

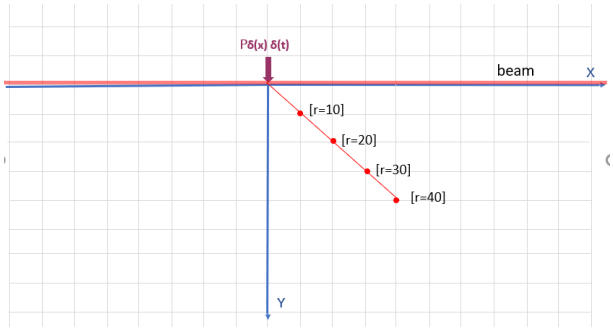

Figure 3.7: Multiple points of interest

Wave	Speed [m/s]	r=10 m	r=20 m	r=30 m	r=40 m
Longitudinal (P)	242.41 m/s	0.041 s	0.082 s	0.124 s	0.165 s
Transverse (S)	129.57 m/s	0.073 s	0.154 s	0.232 s	0.308 s
Surface/Rayleigh (R)	120.01 m/s	0.083 s	0.167 s	0.250 s	0.334 s

Table 3.3: Arrival of waves at Points of interest

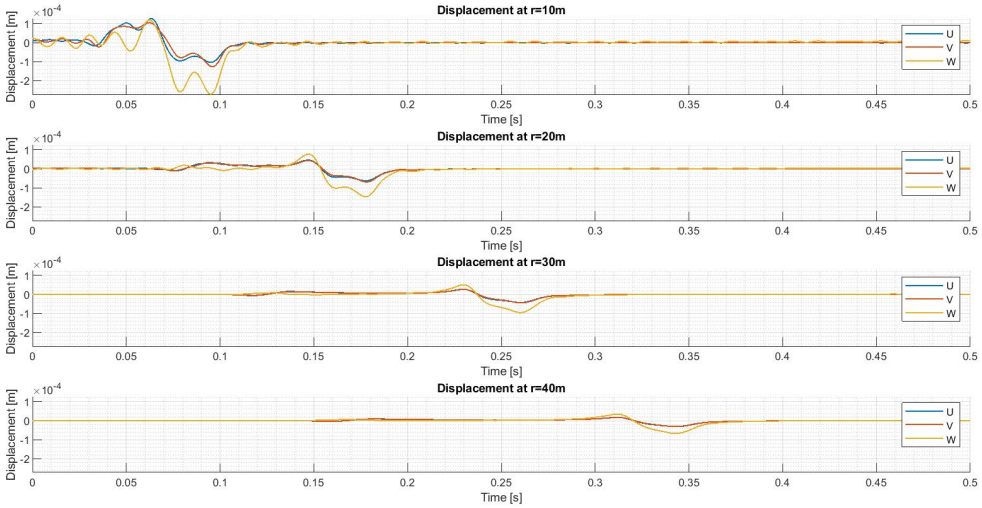

Figure 3.8: Surface displacements at $r = 10, 20, 30, 40$ m

4 LATERAL IMPULSE

This chapter comprises the semi-analytical solution for the displacements and velocities of a half-space when a lateral impulse point force acts on a beam. The interacting forces between beam and half-space are obtained by making use of the equivalent stiffness of the soil. The first system that is solved is an infinite Euler-Bernoulli beam in interaction with frequency-dependent springs, representing the soil. Hereafter the spring forces are taken as excitation force on the soil, spread over the width of the beam. The problem is solved in the frequency domain and the results are analysed in the time domain.
The significant difference between Chapter:3 and Chapter:4 is in the formulation of Lamb scalar wave potentials explained in the following sections.

4.1 MODEL

The model consists of 2 linear sub-domains: Ω_b and Ω_s which refers to the beam and the half-space respectively. [Fig.4.1]

- **Beam(Ω_b)** : A Euler Bernoulli beam of width $2a$ (y-direction) and of infinite length (x-direction) is present on a 3 dimensional half-space(x, y, z). The beam's flexural rigidity (EI) and mass per unit length (m) are assumed to be longitudinally invariant.
- **Half-space(Ω_s)**: The half-space is an elastic, homogeneous and isotropic medium defined by Lamb's equations. (Lamb [1904])
- **Force (F_b)**: An impulse point force of value P is exerted at $t = 0$ on the origin $(0, 0)$ of the beam along y-direction (referred to as lateral) [Eq.4.1]

$$F_b = P\delta(x)\delta(t) \tag{4.1}$$

- **Interaction**: The interaction between the two domains (Ω_b, Ω_s) is achieved through enforcing displacement continuity about the mid-line of the beam and stress continuity over the width of the beam (2a). The linear approach leads to the concept of equivalent stiffness which is the key interaction factor as derived in Dieterman and Metrikine [1996].

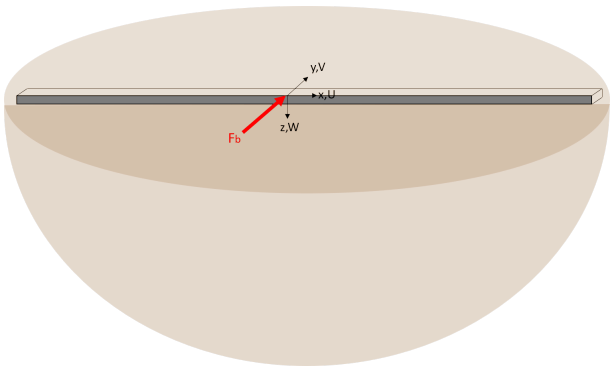

Figure 4.1: Representation of Model -2

4.2 GOVERNING EQUATIONS: SPACE-TIME

Half-space

The equation of motion of the half-space domain (Ω_s) is [Eq.4.2] as expressed by Aki and G.Richards [2002] . The displacement vector is composed of three scalar wave potentials (ϕ, ψ, χ) which co relates to P wave, SV wave and SH wave respectively.

$$\vec{u} = \nabla\phi + \nabla \times \nabla \times (0, 0, \psi) + \nabla \times (0, 0, \chi) \tag{4.2}$$

Where $\vec{u}$ is the displacement vector of the half-space comprising the displacements in (x, y, z) direction respectively as U, V, W. [Eq.4.3]

$$\vec{u}(x, y, z, t) = \{U(x, y, z, t), V(x, y, z, t), W(x, y, z, t)\} \tag{4.3}$$

The equation of motion of the half-space in terms of scalar wave potentials $(\phi, \psi$ & $\chi)$ that represent the three types of waves, P, SV & SH waves respectively are [Eq.4.4-4.6]; where c_l and c_t are the speed of the longitudinal and transverse waves in the half-space respectively.

$$\nabla^2\phi = \frac{1}{c_l^2}\frac{\partial^2\phi}{\partial t^2} \tag{4.4}$$

$$\nabla^2\psi = \frac{1}{c_t^2}\frac{\partial^2\psi}{\partial t^2} \tag{4.5}$$

$$\nabla^2\chi = \frac{1}{c_t^2}\frac{\partial^2\chi}{\partial t^2} \tag{4.6}$$

The displacements (U, V, W) which comprises the vector $\vec{u}$ are notated through scalar wave potentials as [Eq.4.7-4.9]. On an obvious observation, the SH scalar wave potential, χ does not influence the displacement in z-direction, W, which is reasoned through the definition of SH waves as explained in Chapter 2.

$$U = \frac{\partial\phi}{\partial x} + \frac{\partial^2\psi}{\partial x\partial z} + \frac{\partial\chi}{\partial y} \tag{4.7}$$

$$V = \frac{\partial\phi}{\partial y} + \frac{\partial^2\psi}{\partial y\partial z} - \frac{\partial\chi}{\partial x} \tag{4.8}$$

$$W = \frac{\partial\phi}{\partial z} + \frac{\partial^2\psi}{\partial z^2} - \frac{1}{c_{t^2}}\frac{\partial^2\psi}{\partial t^2} \tag{4.9}$$

Beam

The equation of motion of the beam is [Eq.4.10], where V^o is the displacement of the beam in the y-direction, F_s is the interacting force per unit length between the beam and the soil in y-direction and F_b is the force per unit length exerted on the beam by an external source and both the forces are exerted along the y-direction. The characteristics of the beam, m and EI are the mass per unit length and bending stiffness of the beam respectively which are considered to be a constant along it's length and in time.

$$m\frac{\partial^2 V^o}{\partial t^2} + EI\frac{\partial^4 V^o}{\partial x^4} = F_s(x, t, V^o(x, t)) + F_b(x, t) \tag{4.10}$$

The beam is assumed to be of Euler Bernoulli in nature, due to its assumption F_b and F_s are forces per unit length that depends only on x and time.F_s also is interconnected to the displacement of the beam (V^o).

Boundary conditions

The boundary conditions of the half-space at the surface are [Eq.4.11-4.14]. The interacting force, F_s, which in this case is exerted by the beam on the half-space is always in equilibrium with the shear stress on the surface (τ_{yz}) [Eq.4.11]. An important characteristic of the interacting force (F_s) is in its application:

- When exerted by the half-space (Ω_s) on the beam (Ω_b): As explained in sub-section 4.2, it is acting per unit length on the E-B beam incorporated in equation of motion of the beam.
- Whereas when F_s is exerted by the beam (Ω_b) on the half-space (Ω_s): It is smeared uniformly along the width of the beam ($2a$), therefore the Heaviside-function is applicable in linking it against the shear stress(τ_{yz}) in the boundary condition of the half-space[Eq.4.11]. Consequently, the robustness of uniform distribution of stress across $2a$ is acceptable under the clause that the waves in beams have a wavelength much higher than the width of the beam.

The application of F_s, is referred from Dieterman and Metrikine [1996] is for low frequency content. The assumed boundary condition suffices as concluded in Steenbergen and Metrikine [2007].

$$2a\tau_{yz}(x,y,0,t) = F_s(x,t,V^o(x,t)(H(y+a) - H(y-a)) \tag{4.11}$$

As the surface of the half-space does not experience any form of loading apart from that of the beam and it is assumed that the stresses are independent, it can be evaluated that the normal stress on the surface σ_{zz} is zero at all times [Eq.4.12] and similarly, the shear stress along x-direction on the surface τ_{xz} is also zero.[Eq.4.13]

$$\sigma_{zz}(x,y,0,t) = 0 \tag{4.12}$$

$$\tau_{xz}(x,y,0,t) = 0 \tag{4.13}$$

The interface condition between the beam Ω_b and the half-space Ω_s is further linked through the displacement continuity as a linear system is assumed [Eq.4.14]. Therefore the displacements of the beam along y-direction, V^o is equal to the surface displacement of the half-space along y-direction, V at the mid-line of the beam at all times:

$$V(x,0,0,t) = V^o(x,t) \tag{4.14}$$

The stresses expressed in terms of scalar wave potentials which would aid in further simplifications is expressed in [Eq.4.15-4.17]

$$\tau_{yz} = \mu(2\frac{\partial^2\phi}{\partial y\partial z} + 2\frac{\partial^3\psi}{\partial y\partial z^2} - \frac{\partial^3\psi}{c_t^2\partial y\partial t^2} - \frac{\partial^2\chi}{\partial x\partial z}) \tag{4.15}$$

$$\sigma_{zz} = \frac{\lambda}{c_l^2}\frac{\partial^2\phi}{\partial t^2} + 2\mu(\frac{\partial^2\phi}{\partial z^2} + \frac{\partial^3\psi}{\partial z^3}) - 2\rho\frac{\partial^3\psi}{\partial z\partial t^2} \tag{4.16}$$

$$\tau_{xz} = \mu(2\frac{\partial^2\phi}{\partial x\partial z} + 2\frac{\partial^3\psi}{\partial x\partial z^2} - \frac{\partial^3\psi}{c_t^2\partial x\partial t^2} + \frac{\partial^2\chi}{\partial y\partial z}) \tag{4.17}$$

4.3 GOVERNING EQUATIONS – WAVENUMBER–FREQUENCY DOMAIN

4.3.1 Forward Fourier Transform

The governing equations of motion described in section 4.2 is transformed to wavenumber-frequency domain as [Eq.4.18], where k_1, k_2 are the wavenumbers and ω is the angular frequency:

$$F(k_1,k_2,z,\omega) = \int_{-\infty}^{\infty}\int_{-\infty}^{\infty}\int_{-\infty}^{\infty} f(x,y,z,t)e^{i(\omega t - k_1 x - k_2 y)}dtdxdy \tag{4.18}$$

On fourier transforming the governing equations, the notations of relevant terms are expressed in Table:4.1.

Name	Space-Time	Wavenumber-Frequency
P-wave scalar potential	$\phi(x,y,z,t)$	$f(k_1,k_2,z,\omega)$
SV-wave scalar potential	$\psi(x,y,z,t)$	$g(k_1,k_2,z,\omega)$
SH-wave scalar potential	$\chi(x,y,z,t)$	$h(k_1,k_2,z,\omega)$
Displacement of beam	$V^o(x,t)$	$p(k_1,\omega)$
Force on beam	$F_b(x,t)$	$\tilde{f}_b(k_1,\omega)$
Interacting force	$F_s(x,t,V^0(x,t))$	$\tilde{f}_s(k_1,\omega,p(k_1,\omega))$

Table 4.1: Fourier Transform notation

4.3.2 Governing Equations

The equations of motion of the half-space in terms of scalar wave potentials derived from [Eq.4.4-4.6] are [Eq.4.27-4.29] in the wavenumber-frequency domain, where c_l and c_t are the speeds of longitudinal and transverse waves respectively:

$$\frac{\partial^2 f}{\partial z^2} + (\frac{\omega^2}{c_l^2} - k_1^2 - k_2^2)f = 0 \tag{4.19}$$

$$\frac{\partial^2 g}{\partial z^2} + (\frac{\omega^2}{c_t^2} - k_1^2 - k_2^2)g = 0 \tag{4.20}$$

$$\frac{\partial^2 h}{\partial z^2} + (\frac{\omega^2}{c_t^2} - k_1^2 - k_2^2)h = 0 \tag{4.21}$$

The equation of motion of the beam following from [Eq.4.10] is derived as [Eq.4.22] in wavenumber-frequency domain:

$$p(\omega,k_1)D(\omega,k_1) = \tilde{f}_s(\omega,k_1,p(\omega,k_1)) + \tilde{f}_b(\omega,k_1) \tag{4.22}$$

Where $D(\omega,k_1) = -m\omega^2 + EIk_1^4$ is the dispersion equation of the beam.
The boundary conditions of the half-space [Eq.4.11-4.14] on transforming to the wavenumber-frequency domain are respectively:

$$i\mu(-2k_2\frac{\partial f}{\partial z} - 2k_2\frac{\partial^2 g}{\partial z^2} - k_2\frac{\omega^2}{c_t^2}g + k_1\frac{\partial h}{\partial z}) = \tilde{f}_s(\omega,k_1,p(\omega,k_1))\frac{sin(ak_2)}{ak_2} \tag{4.23}$$

$$-\frac{\lambda}{c_l^2}\omega^2 + 2\mu(\frac{\partial^2 f}{\partial z^2} + \frac{\partial^3 g}{\partial z^3}) + 2\rho\omega^2\frac{\partial \psi}{\partial z} = 0 \tag{4.24}$$

$$i\mu(-2k_1\frac{\partial f}{\partial z} - 2k_1\frac{\partial^2 g}{\partial z^2} - k_1\frac{\omega^2}{c_t^2}g - k_2\frac{\partial h}{\partial z}) = 0 \tag{4.25}$$

The interface condition [Eq.4.14] is fourier transformed as [Eq.4.26]. :

$$p(\omega,k_1) = \frac{1}{2\pi}\int_{-\infty}^{\infty} v(k_1,k_2,0,\omega)dk_2 \tag{4.26}$$

Where $v(k_1,k_2,z,\omega) = \int_{-\infty}^{\infty}\int_{-\infty}^{\infty}\int_{-\infty}^{\infty} V(x,y,z,t)e^{i(\omega t - k_1 x - k_2 y)}dtdxdy$ where V is the displacement in y-direction of the half-space [Eq.4.8]. The wavenumber-frequency domain expression of V is convoluted across k_2 domain in order to interconnect the midline displacement of the beam to the half-space in [Eq.4.26]

4.4 SOLUTION TO GOVERNING EQUATIONS

Owing to the characteristics of a half-space, the equations of motion corroborating with Sommerfield's radiation condition is [Eq. 4.27-4.29]:

$$f = A(k_1,k_2,\omega)e^{-zR_l} \tag{4.27}$$

$$g = B(k_1, k_2, \omega)e^{-zR_t} \tag{4.28}$$

$$h = C(k_1, k_2, \omega)e^{-zR_t} \tag{4.29}$$

Where A, B and C are viewed as horizontal wave functions as described by Aki and G.Richards [2002] as they hold the information of the wave potential along k_1, k_2 and do not depend on z-direction. A, B and C also correspond to P, SV and SH wave potentials respectively on the surface $z = 0$. The exponent is the function that prescribes the wave potential's value along z-direction, therefore $R_{l,t}$ is [Eq.4.30] :

$$R_{l,t} = \begin{cases} \sqrt{(k_1^2 + k_2^2) - \frac{\omega^2}{c_{l,t}^2}} & \text{if } \frac{\omega^2}{c_{l,t}^2} < k_1^2 + k_2^2 \\ i\sqrt{\frac{\omega^2}{c_{l,t}^2} - (k_1^2 + k_2^2)} & \text{if } \frac{\omega^2}{c_{l,t}^2} > k_1^2 + k_2^2 \end{cases} \tag{4.30}$$

On substituting the equation of motion of half-space [Eq.4.27-4.29] in the boundary conditions [Eq.4.23-4.26], linear equations obtained are which are then solved for A, B and C as [Eq.4.31-4.33] :

$$A = 2i\tilde{f}_s R_t \frac{sin(ak_2)}{a\mu\Delta} \tag{4.31}$$

$$B = i\tilde{f}_s \frac{(2R_t^2 + \frac{\omega^2}{c_t^2})}{(k_1^2 + k_2^2)} \frac{sin(ak_2)}{a\mu\Delta} \tag{4.32}$$

$$C = i\tilde{f}_s \frac{k_1}{(R_t(k_1^2 + k_2^2))} \frac{sin(ak_2)}{a\mu k_2} \tag{4.33}$$

Where,

$$\Delta = (2(k_1^2 + k_2^2) - \frac{\omega^2}{c_t^2})^2 - 4R_l R_t (k_1^2 + k_2^2) \tag{4.34}$$

4.4.1 Equivalent Stiffness

In order to find the interaction force F_s, it is essential to solve for equivalent stiffness of the interaction between the beam and the half-space.Therefore, it is assumed that no external load acts and proceed by solving the interface condition [Eq.4.26].The wavenumber-frequency domain expression of the half-space displacement along y-direction is [Eq.4.35]

$$v(k_1, k_2, z, \omega) = -i[k_2(f + \frac{\partial g}{\partial z}) - k_1 h] \tag{4.35}$$

The beam's equation of motion when $F_b = 0$ is [Eq.4.36] :

$$\tilde{f}_s(\omega, k_1, p(\omega, k_1)) = p(\omega, k_1)D(\omega, k_1) \tag{4.36}$$

On substituting the expressions of f, g and h from [Eq.4.31-4.33] at $z = 0$ in [Eq.4.35], leads to the value of v as expressed in [Eq.4.37].

$$v(k_1, k_2, 0, \omega) = \frac{p(\omega, k_1)D(\omega, k_1)}{\mu R_t} \frac{(k_2^2 R_t^2 \frac{\omega^2}{c_t^2} - k_1^2\Delta)}{(k_1^2 + k_2^2)\Delta} \frac{sin(ak_2)}{ak_2} \tag{4.37}$$

Substituting [Eq.4.37] in [Eq.4.26] :

$$p(\omega, k_1)\left\{1 - \frac{D(\omega, k_1)}{2\pi\mu}\int_{-\infty}^{\infty} \frac{(k_2^2 R_t^2 \frac{\omega^2}{c_t^2} - k_1^2\Delta)}{R_t(k_1^2 + k_2^2)\Delta} \frac{sin(ak_2)}{ak_2} dk_2\right\} = 0 \tag{4.38}$$

The equation above, [Eq.4.38] can also be viewed as: $p(\omega,k_1)D(\omega,k_1)+\chi(\omega,k_1)=0$ and with reference to Dieterman and Metrikine [1996] the equivalent stiffness of the half-space is χ from the mentioned form of equation.Therefore, the equivalent stiffness χ can be derived as [Eq.4.39].

$$\chi(\omega,k_1)=-2\pi\mu\left(\int_{-\infty}^{\infty}\frac{(k_2^2R_t^2\frac{\omega^2}{c_t^2}-k_1^2\Delta)}{R_t(k_1^2+k_2^2)\Delta}\frac{sin(ak_2)}{ak_2}dk_2\right)^{-1} \tag{4.39}$$

Where $\Delta(k_1,k_2,\omega)=(2(k_1^2+k_2^2)-\frac{\omega^2}{c_t^2})^2-4R_lR_t(k_1^2+k_2^2)$ and $R_{l,t}$ follows the condition in [Eq.4.30].

4.4.2 Interaction force

From the equivalent stiffness derived in [Eq.4.39] for a case of no external loading, the interaction force is rephrased as expressed in [Eq.4.40]:

$$\begin{aligned}\tilde{f_s}&=h(\omega,k_1)D(\omega,k_1)\\ \text{Also}:\ &h(\omega,k_1)(D(\omega,k_1)+\chi(\omega,k_1))=0\\ \text{Therefore}:\ &\tilde{f_s}=-h(\omega,k_1)\chi(\omega,k_1)\end{aligned} \tag{4.40}$$

Similarly, for the case of an external loading existing, the equations can be re-phrased, to find the interaction force as [Eq.4.41]:

$$\begin{aligned}h(\omega,k_1)(D(\omega,k_1)+\chi(\omega,k_1))&=\tilde{f}_b(\omega,k_1)\\ \text{Therefore}:\ \tilde{f_s}&=-\frac{\tilde{f}_b(\omega,k_1)\chi(\omega,k_1)}{D(\omega,k_1)+\chi(\omega,k_1)}\end{aligned} \tag{4.41}$$

4.5 SURFACE DISPLACEMENT

The displacements of the half-space in the wave-number frequency domain are [Eq.4.42]:

$$\begin{aligned}\tilde{u}&=-ik_1(f+\frac{\partial g}{\partial z})-ik_2h\\ \tilde{v}&=-ik_2(f+\frac{\partial g}{\partial z})+ik_1h\\ \tilde{w}&=\frac{\partial f}{\partial z}+\frac{\partial^2 g}{\partial z^2}+\frac{\omega^2}{c_t^2}g\end{aligned} \tag{4.42}$$

At the surface, $z=0$, the displacements are [Eq.4.43]:

$$\begin{aligned}\tilde{u}&=\frac{\tilde{f_s}}{\mu R_t\Delta}\frac{k_1k_2(R_t^2\frac{\omega^2}{c_t^2}-\Delta)}{(k_1^2+k_2^2)}\frac{sin(ak_2)}{ak_2}\\ \tilde{v}&=\frac{\tilde{f_s}}{\mu R_t\Delta}\frac{(k_2^2R_t^2\frac{\omega^2}{c_t^2}-k_1^2\Delta)}{(k_1^2+k_2^2)}\frac{sin(ak_2)}{ak_2}\\ \tilde{w}&=-\frac{\omega^2}{c_t^2}R_l\frac{\tilde{f_s}}{\mu\Delta}\frac{sin(ak_2)}{ak_2}\end{aligned} \tag{4.43}$$

Where $\Delta(k_1,k_2,\omega)=(2(k_1^2+k_2^2)-\frac{\omega^2}{c_t^2})^2-4R_lR_t(k_1^2+k_2^2)$ and $R_{l,t}$ follows the condition in [Eq.4.30], and $\tilde{f_s}$ is given by [Eq.4.41].

4.5.1 Inverse Fourier Transform

Inverse fourier transform of surface displacements [Eq.4.43] from the wavenumber-frequency domain to the frequency domain are [Eq. 4.44]. By transforming the expressions to the frequency domain, it can then be further transformed to the time domain in order to view the ground displacements as a function of space and time.

$$\begin{aligned}
\tilde{U}(x,y,0,\omega) &= \frac{1}{4\pi^2}\int_{-\infty}^{\infty}\int_{-\infty}^{\infty}\frac{\tilde{f}_s}{\mu R_t \Delta}\frac{k_1 k_2(R_t^2\frac{\omega^2}{c_t^2}-\Delta)}{(k_1^2+k_2^2)}\frac{sin(ak_2)}{ak_2}e^{ik_1x+ik_2y}dk_1dk_2 \\
\tilde{V}(x,y,0,\omega) &= \frac{1}{4\pi^2}\int_{-\infty}^{\infty}\int_{-\infty}^{\infty}\frac{\tilde{f}_s}{\mu R_t \Delta}\frac{(k_2^2R_t^2\frac{\omega^2}{c_t^2}-k_1^2\Delta)}{(k_1^2+k_2^2)}\frac{sin(ak_2)}{ak_2}e^{ik_1x+ik_2y}dk_1dk_2 \\
\tilde{W}(x,y,0,\omega) &= \frac{1}{4\pi^2}\int_{-\infty}^{\infty}\int_{-\infty}^{\infty}-\frac{\omega^2}{c_t^2}R_l\frac{\tilde{f}_s}{\mu\Delta}\frac{sin(ak_2)}{ak_2}e^{ik_1x+ik_2y}dk_1dk_2
\end{aligned} \tag{4.44}$$

The last step is to obtain the time domain displacements, and [Eq.4.44] are inverse fourier transformed again as [Eq. 4.45] to the time domain.

$$\begin{aligned}
U(x,y,0,t) &= \frac{1}{2\pi}\int_{-\infty}^{\infty}\tilde{U}(x,y,0,\omega)e^{-i\omega t}d\omega \\
V(x,y,0,t) &= \frac{1}{2\pi}\int_{-\infty}^{\infty}\tilde{V}(x,y,0,\omega)e^{-i\omega t}d\omega \\
W(x,y,0,t) &= \frac{1}{2\pi}\int_{-\infty}^{\infty}\tilde{W}(x,y,0,\omega)e^{-i\omega t}d\omega
\end{aligned} \tag{4.45}$$

4.5.2 Numerical Solution-MATLAB

The surface displacements are calculated and inverse fourier transformed numerically using MATLAB. Table-4.2 are the model details considered as input with reference to Dieterman and Metrikine [1996]. A damping of 5% is provided in the shear modulus of the half-space.

Domain	Name	Value	Unit
Half-space	Shear Modulus of half-space (μ)	3.27×10^7	N/m^2
	Poisson's Ratio (ν)	0.3	
	Material Damping	2.5%	
	Density of half-space (ρ)	1960	kg/m^3
	Longitudinal wave speed (c_l)	$242.34 + 6.05i$	m/s
	Transverse wave speed (c_t)	$119.97 + 2.99i$	m/s
	Rayleigh wave speed (c_r)	$129.54 + 3.23i$	m/s
Beam	Mass of beam (m)	760	kg/m
	Flexural Rigidity (EI)	1.29×10^7	Nm^2
	Width of beam (a)	2.6	m
Force	Axle load on beam (F_b)	$225\delta(x)\delta(t)$	kN

Table 4.2: Numerical Model Details

4.6 RESULT

For the given problem statement of an impulse point load, the points of discussion that is vital for understanding the problem and the solution are:

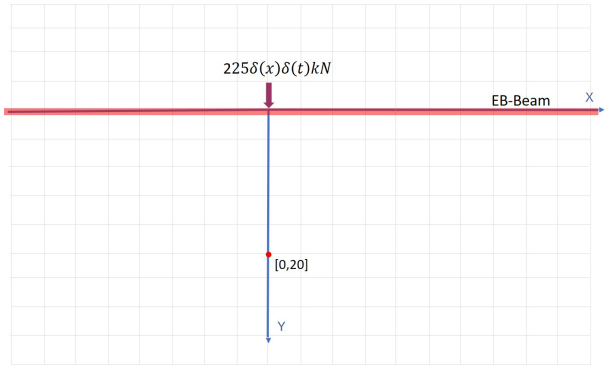

Figure 4.2: Model and Point of interest

- The interacting force (F_s): For an impulse that is applied, F_s is analysed for multiple frequencies, to notice how it behaves in the space domain. This is the loading problem on the half-space. The spatial as well as time smearing nature of the interacting force, is essential in a railway schematic problem.
- The surface displacements (U, V, W): The displacements in the frequency domain as well as time domain is essential to notice as this is the solution and key in analysing the ground vibrations.

The ground vibrations are also analysed in particular to the point of interest as depicted in [Fig.4.2].

4.6.1 Interacting force

The interacting force, [Eq.4.41] is a function of the applied load ($\tilde{f}_b$), the equivalent stiffness between the domains (χ) and the dispersion equation of the beam (D) in the wavenumber-frequency domain. For a loading force of $F_b = 225kN\delta(x)\delta(t)$, the interacting force is derived in the frequency-wavenumber domain and fourier transformed to the frequency-space domain to analyse the spread of the force across the beam and in the half-space ($2a$). It is to be noted that since the applied load is an impulse, in the frequency domain it is a constant ($\tilde{f}_b = 225$), thus activating all frequencies of loads.

The interaction force (F_s) is analysed in [Fig.4.3] as a ratio to the magnitude of the loading force ($225KN$) and its spread along x axis. The force(F_s) is analysed at three different loading force frequency: 5, 25, 50 Hz applied at the origin $(0, 0)$. The points to observe from the [Fig.4.3] are:

- At $5Hz$, the magnitude of the force is maximum and reduces at $25Hz$ and further at 50 Hz. This is because the interaction force is a form of response by the half-space to the loading on the beam, therefore, when the loading frequency is high, the response does not acquire sufficient time to absorb the entirety of the loading energy to respond. This conclusively means, when the loading frequency is 0, that is when a stationary load is applied, then the response, (F_s) will be of equal and opposite value.
- At $5Hz$ the force dampens out quickly, whereas at increasing frequencies, the spread of the force across the beam increases.It can be viewed at a perspective that for a given load energy, at multiple frequencies the spread of the resisting force is accordingly, that the total energy is equal.

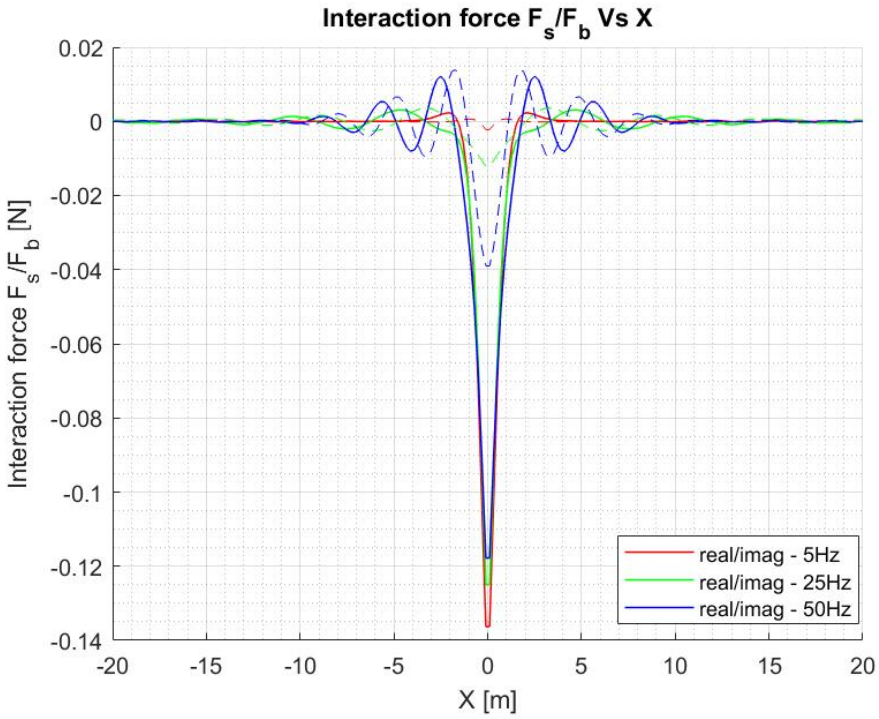

Figure 4.3: Interaction force at 5, 25 and 50 Hz of Loading force (F_b) frequency

4.6.2 Surface displacements

The displacements at z=0, is found from the Eq.4.44 on numerically integrating them. Fig.4.4 contains the displacements(U, V, W) along y=0, i.e. right under the mid-line of the beam, for three different loading force frequencies ($5, 25, 50Hz$).The points to observe from the figure are:

- U, W are almost 0 across the x-axis, and V is symmetric across the x-axis with the maximum value under the point of loading. Theoretically, the value of V under the point of loading is infinite because it is a singular load on a half-space, right under the nose of the loading.
- For a loading frequency of $5Hz$, magnitude of V is higher than in $25Hz$ and $50Hz$, this is because the response does not acquire sufficient time to absorb the loading force at higher frequencies. However, the total energy imparted and responded would be equal for all frequencies.

In Fig.4.5 the displacements along y=10, i.e. 10 m away from the beam are derived. The points to observe from the figure are:

- U has an anti-symmetric mode of vibration and this is due to the symmetry of the half-space and the load. V, W have symmetric mode of vibration across the y-axis.
- U is 0 along the y-axis, where as V, W reach the maximum value along the y-axis, the direction of load. This is also due to symmetry that the value of x-direction displacement is 0 along the y-axis. Whereas, V, W have higher displacements as the load is along the y-direction and on the surface of the half-space.
- The values of displacements are higher at a lower loading frequency of $5Hz$ when compared to higher frequencies. The reason to this is mentioned previously.

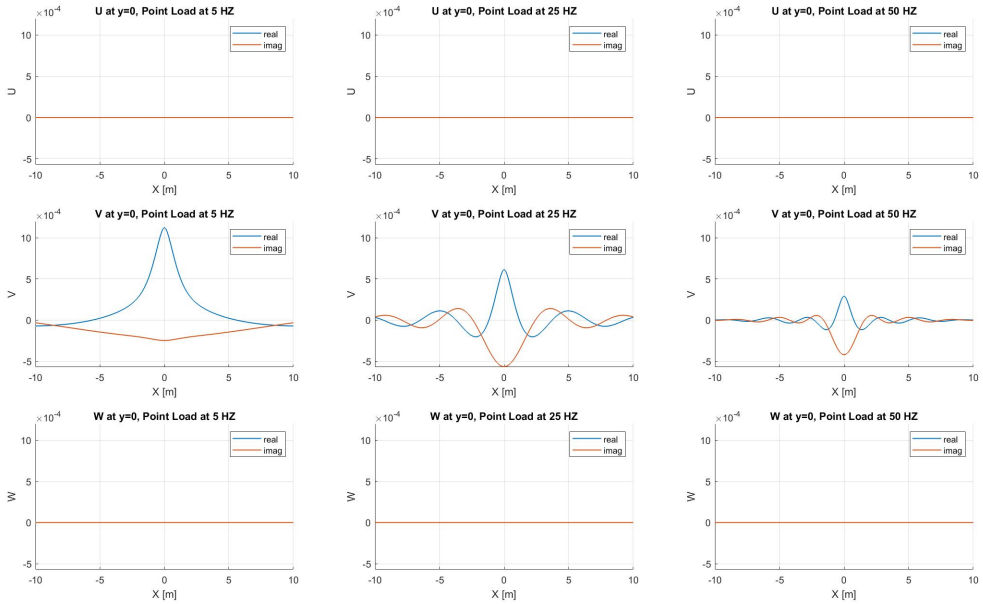

Figure 4.4: Surface displacements at y=0 when loading frequency is 5,25 and 50 Hz

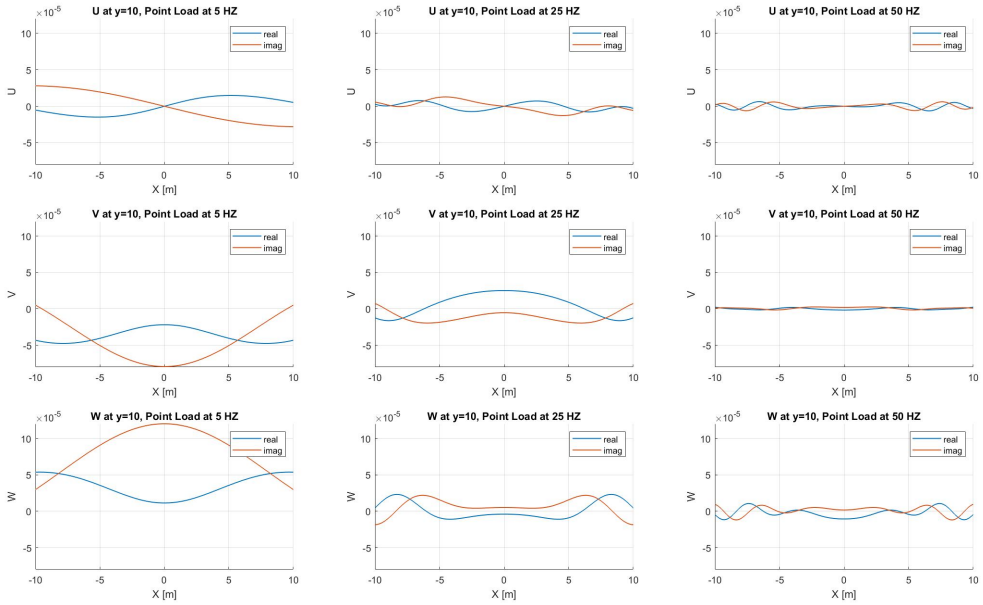

Figure 4.5: Surface displacements at y=10 when loading frequency is 5,25 and 50 Hz

Point of Interest

For the POI $[0, 20]$ the surface displacements are derived in wavenumber-frequency domain and consequently fourier transformed to space-time domain. For the provided model details, analytically the speeds of the longitudinal,transverse and rayleigh waves are calculated and the arrival time of these waves is thus estimated for the distance between the load and POI $(20m)$. [4.4]

Name	Speed [m/s]	Arrival time [s]
P-wave	$242.41 m/s$	$0.082 s$
S-wave	$129.57 m/s$	$0.154 s$
R-wave	$120.08 m/s$	$0.166 s$

Table 4.3: Estimated Arrival time of waves at [0,20]

The numerical model derived ground vibration at POI is expressed in the frequency and time domain in [Fig.4.6]. It can be observed that the model is in co-ordination with the estimated arrival time of waves. The P-waves arrive first, followed by the S-waves and the surface waves (R-waves) arrive at the end. The disturbance at time $t = 0$ is due to numerical truncation limit in the frequency domain.

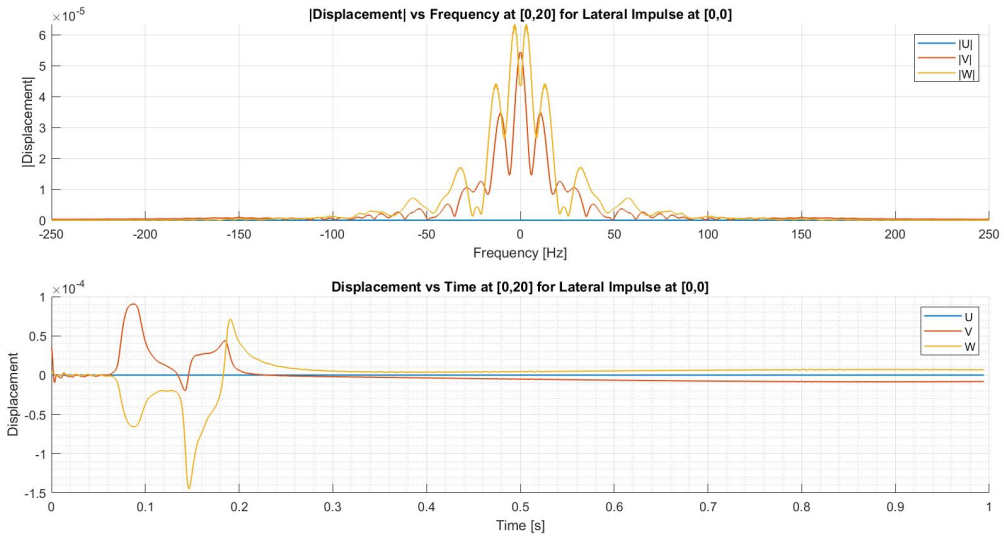

Figure 4.6: Surface velocity at [0,20] in frequency and time domain

4.6.3 Multiple points of interest

Diagonally from the point of loading, four points of interest are considered with radial distances of 10, 20, 30, 40 m on the surface [Fig.4.7]. The displacements at these points are plotted for an impulse point load at the origin on the beam [Fig.4.8]. The arrival of waves is calculated from the speeds in Table:4.4. The points to notice are:

- The attenuation in waves along the distance is observed from the magnitude of displacements
- U, V are almost equal for higher distances, which can be inferred that at higher distances the beam's influence is reduced. Whereas, at $r = 10$ m, the values of U, V are different.
- The P-wave arrival is significant in U, V when compared to W as they are significant in along the surface direction.
- The time difference between the arrival of P-wave and surface waves is higher for higher distances.

Wave	Speed [m/s]	r=10 m	r=20 m	r=30 m	r=40 m
Longitudinal (P)	242.41 m/s	0.041 s	0.082 s	0.124 s	0.165 s
Transverse (S)	129.57 m/s	0.073 s	0.154 s	0.232 s	0.308 s
Surface/Rayleigh (R)	120.01 m/s	0.083 s	0.167 s	0.250 s	0.334 s

Table 4.4: Arrival of waves at Points of interest

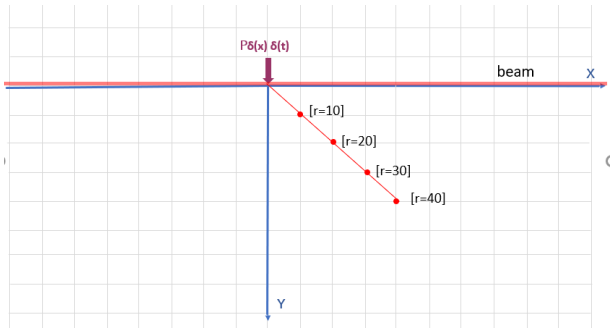

Figure 4.7: Multiple points of interest

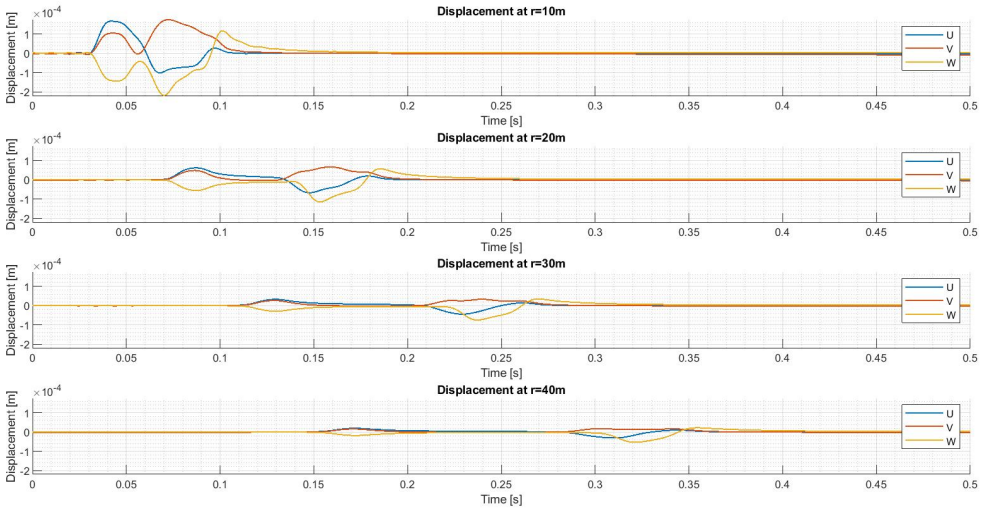

Figure 4.8: Surface displacements at $r = 10, 20, 30, 40$ m

5 TURNOUT

5.1 NUMERICAL – MODEL

A standard railway turnout [Fig.5.1] consists of three sections: the switch panel, closure panel and crossing panel. These three sections produce a different type of loading on the soil when a train encounters it. The factors that influence the magnitude of the loading are varied from speed of the train, wheel-set of the train, dip angle in the railway track, change in stiffness of the tracks through the three sections, soil properties, effect of sleepers and ballast, wear and tear level of the tracks and wheels, main or branch line encounter of the train, left or right wheel etc.

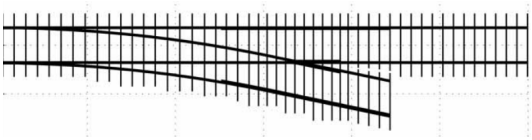

Figure 5.1: A standard turnout

The numerical model depicting a railway turnout setup is simplified through the following assumptions:

- The magnitude of the loading function on the railway tracks depends only on the longitudinal position of the train's wheel-set. The vertical and lateral forces occurring in a turnout are considered whereas the longitudinal forces occurring are out of scope. Although multiple factors affect the magnitude of the loads, the overall behaviour of the loading function is similar as described in Chapter:2.
- The turnout track system is considered as a two-dimensional Euler-Bernoulli beam. Therefore, irrespective of the train encountering the main or branch line of the turnout, the track system is modelled similarly.

The numerical model of a train going through a railway turnout is therefore built up from the building blocks which are Model-1 derived in Chapter:3 for a point impulse load applied vertically and Model-2 derived in Chapter:4 for a point impulse load applied laterally. The following modifications are performed to build the turnout model [Fig.5.2]:

1. The Euler-Bernoulli beam which represents the tracks of the turnout system, are discretised along the length of the beam.
2. The loading is executed as a series of impulses applied at points of discretisation along the beam at different time instances with different magnitudes, thus representing a moving varying load.
3. From Eq.[3.39-3.40] & Eq.[4.44-4.45] the green's function of the displacements at any point is derived when the magnitude of the impulse P is set to unit value, $P = 1$ N. By superposition of the green's function the total displacement at a point can be found. This is further explained in Section.5.2

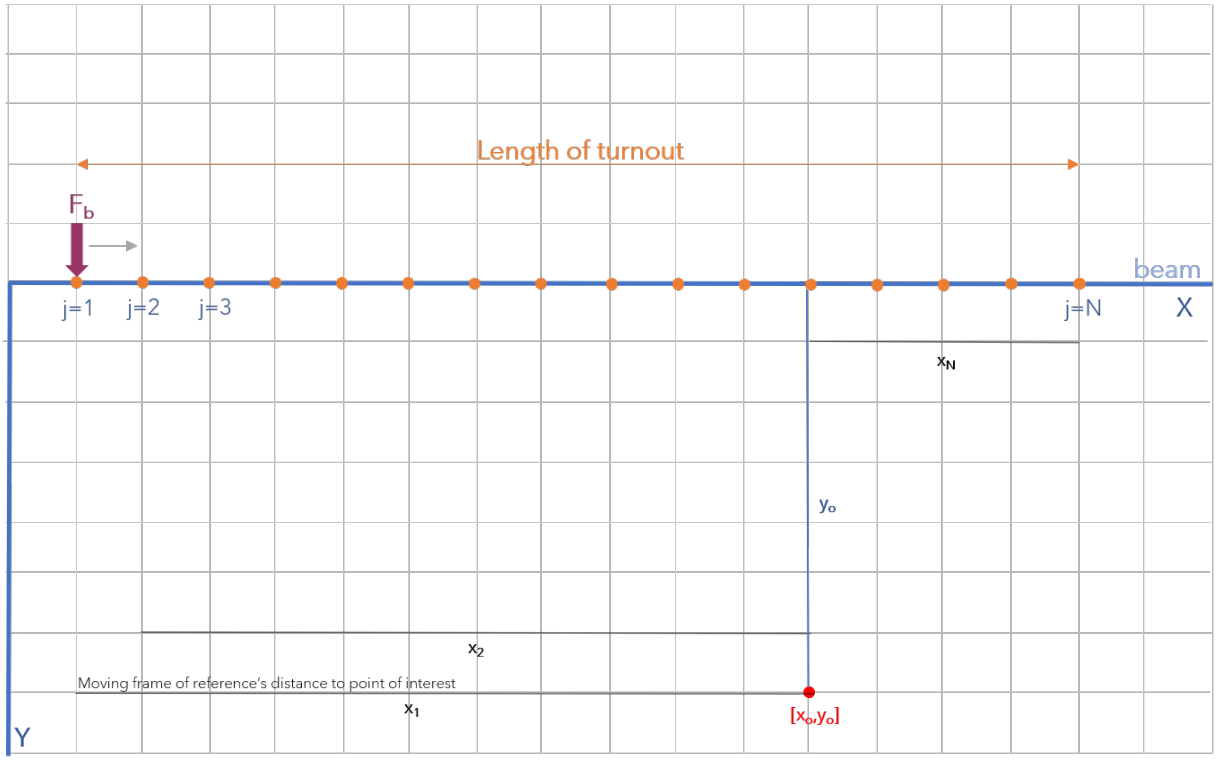

Figure 5.2: Numerical Model for a moving load

5.2 SURFACE VIBRATION

Let the point of interest at which the surface displacements/velocities are to be found be $[0, 20]$ [Fig.5.3 for a turnout like loading function on the beam along x-axis. Let the turnout be of length 20 m spanning from $[-10, 0]$ to $[10, 0]$ and let the loading function exists only within this span of the infinitely long beam. In order to derive the surface vibration the following process is important to understand which is described in the following sections:

- Applying the loading function in the model
- Finding the surface vibrations

5.2.1 Loading Function

The moving load is analytically represented by [Eq.5.1], where c is the speed of the moving load:

$$F_b(x,t) = P(x)\delta(x - ct) \tag{5.1}$$

For a numerical model, the above equation is discretized as [Eq.5.2] where the load moves a length of L which is discretised into N points. The point of application of load is referred to by x_j which is applied at time t_j and are related by the speed of the moving load, c [Eq.5.3] :

$$F_b(x,t) = \sum_{j=1}^{j=N} P_j\delta(x - x_j) \tag{5.2}$$

Where,

$$x_j = ct_j \tag{5.3}$$

In [Eq.5.2], the impulse is applied at $x = x_j$ with respect to space, where as with regards to time it is applied at $t = t_j$.This is because the load acts at x_j at an instant of time t_j which are inter connected

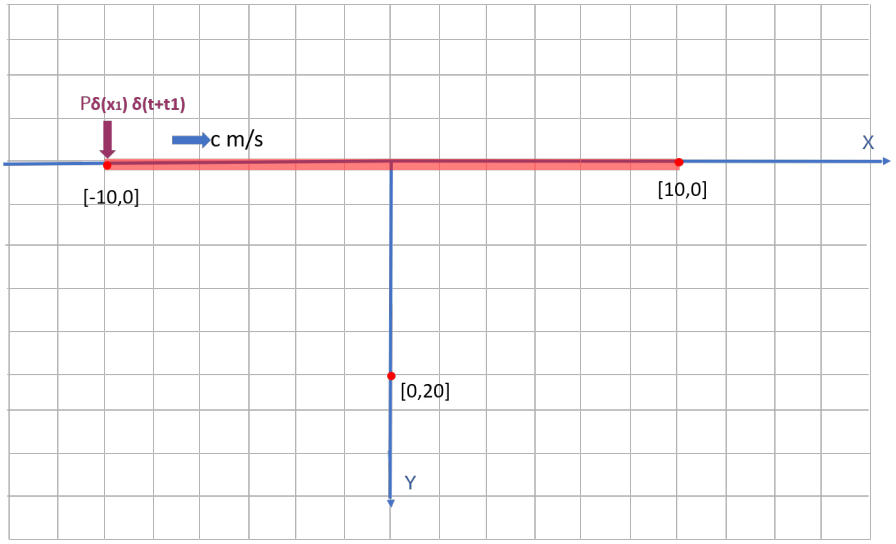

Figure 5.3: Moving load model for the Point of interest [0,20]

through the speed c. This forms a series of impulses acting in space with a delay in time according to the speed considered.
For the given numerical model, the span is of 20 m in length with 201 points in between and the speed is arbitrarily considered as c. There are two load combinations considered:

- Load 1: A constant magnitude of 1 N moving load across the turnout length.[Fig.5.4]
- Load 2: A constant magnitude of 1 N moving load but for the origin, where the load spikes to 2 N. This loading setup is similar to what happens near a crossing, and observing this leads to an insight of response when a sudden defect like encounter occurs between the wheel and the rails.[Fig.5.4]

The loading functions described above are assumed for the case of a vertical force as well as lateral force.

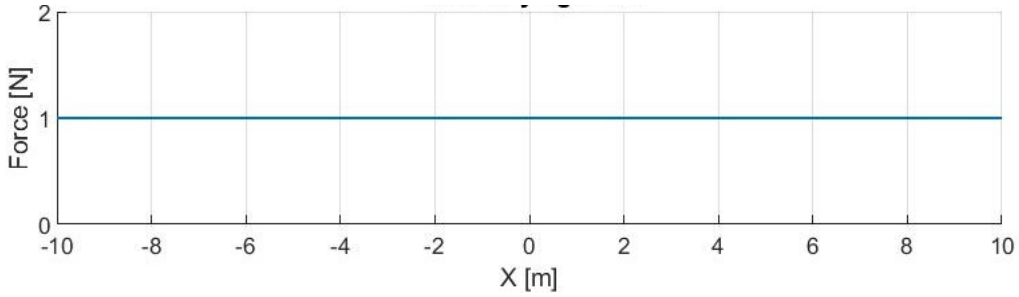

Figure 5.4: Load 1: Constant value load moving along X

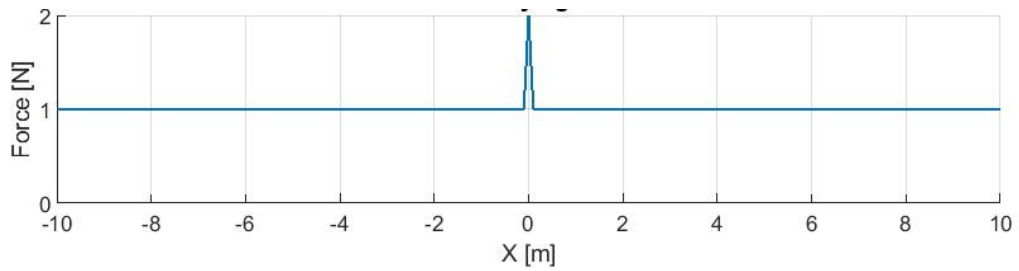

Figure 5.5: Load 2: Varying load moving along X

5.2.2 Surface vibration

- From Eq.[3.39] & Eq.[4.44] the green's function of displacements at any point of interest can be found by evaluating the functions at impulse magnitude, $P = 1$. Let the green's function of displacement be referred by $\vec{\bar{u}}_{gV,L}(x, y, 0, \omega)$ the case of a vertical and lateral impulse point load respectively.
- The time-domain response of the green's function is therefore fourier transformed as [Eq.5.4]

$$\vec{u}_{gV,L}(x_o, y_o, t) = \frac{1}{2\pi}\int_{-\infty}^{\infty} \vec{\bar{u}}_{gV,L}(x, y, 0, \omega)e^{-i\omega t}d\omega \tag{5.4}$$

- The load on the beam, as described above is a moving impulse load with varying magnitude, P(x) moving at speed c [m/s] [Eq.5.5]

$$F_{b_{V,L}}(x, t) = P_{V,L}(x)\delta(x - ct) \tag{5.5}$$

- The surface displacement caused by the moving impulse is perceived as a convolution of the responses from the impulses from moving coordinates and time as described in [Eq.5.6] if the time domain green's function is considered. The convolution, is a form of superposition of the responses from sources of loading at varying coordinates through space and time. This is considered so because, a load that is moving creates a source of excitation as it moves at every coordinate and with speed based time signature and as the system is linear, a superposition of all the responses would lead to the final and total response at any time(t):

$$\vec{u}_{V,L}(x_o, y_o, t) = \int_0^t \int_{-\infty}^{\infty} P_{V,L}(x)\delta(x - c\tau)\vec{u}_{g_{V,L}}(x_o - x, y_o, t - \tau)dxd\tau \tag{5.6}$$

The integration along time (τ) is simplified when the dirac delta function takes the value of 1 which is achieved at:

$$x = c\tau \tag{5.7}$$

Therefore, the displacements can be thus be simplified as [Eq.5.8]:

$$\vec{u}_{V,L}(x_o, y_o, t) = \int_0^{ct} \frac{1}{c}P(x)\vec{u}_{g_{V,L}}(x_o - x, y_o, t - \frac{x}{c})dx \tag{5.8}$$

- Alternatively, if the approach is achieved through frequency domain based green's function, the convolution to achieve the total response is [Eq.5.9]:

$$\vec{u}_{V,L}(x_o, y_o, t) = \frac{1}{2\pi}\int_0^t \int_{-\infty}^{\infty} P_{V,L}(c\tau)\vec{\bar{u}}_{g_{V,L}}(x_o - c\tau, y_o, \omega)e^{-i\omega(t-\tau)}d\omega d\tau \tag{5.9}$$

- Approaching the convolution numerically from [Eq.5.6], the source of loading is constricted to a domain which starts at $x = x_1$ and progresses to $x = x_N$, the loading beyond this domain is neglected. Therefore, the numerical integration is performed through rectangular integration as expressed in [Eq.5.10]:

$$\vec{u}_{V,L}(x_o, y_o, t) = \sum_{j=1}^{N} \frac{1}{c}P(x_j)\vec{u}_{g_{V,L}}(x_o - x_j, y_o, t - t_j)\Delta x \tag{5.10}$$

Where the relation between the space time array is interlinked through speed of load as:

$$(x_j - x_1) = ct_j \tag{5.11}$$

It is also assumed that the loading starts at time, $t_1 = 0$ when the load is at x_1.

- The total displacement is the superposition of the displacements caused by vertical and lateral loading [Eq.5.12].

$$\vec{u}(x_o, y_o, t) = \vec{u}_V(x_o, y_o, 0, t) + \vec{u}_L(x_o, y_o, 0, t) \tag{5.12}$$

5.3 RESULT

5.3.1 Load combinations

The load combinations are based on magnitude of the impulse and it's direction. From section 5.2.1 two load combinations based on magnitude are considered: load 1, where a constant magnitude of 1 N impulse moves along the length of the beam and load 2, where a constant magnitude of 1 N impulse moves except at the origin the magnitude spikes to 2 N. Based on direction of the load, two types are considered which are vertical (z-direction) and lateral (y-direction) load.

These load combinations move at a speed of 10 m/s along the beam length and the velocities generated at a point of interest ($[0, 20]$) is plotted for the combination of load magnitude 1 & 2 and load direction vertical and lateral.

In [Fig.5.6] the arrival of the waves (calculated from the speeds of the waves in soil) to the point of interest is plotted with the P-wave arriving the earliest at $0.092s$ and the surface wave (Rayleigh/R-wave) arriving at the last at $2.18s$. The arrival time of the wave is irrespective of the magnitude and direction of the loads.

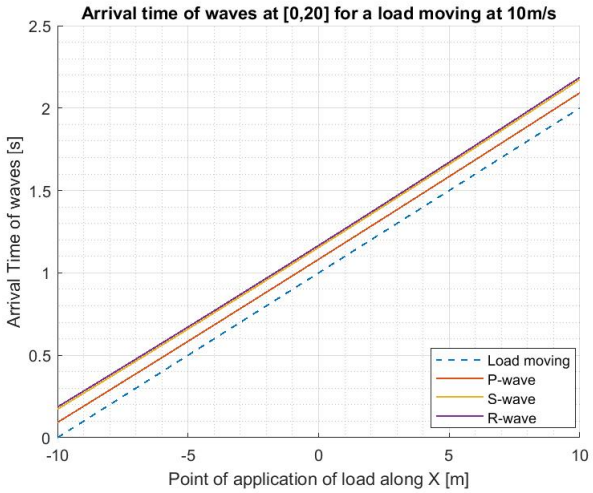

Figure 5.6: Arrival time of waves at [0,20] for a load moving at 10 m/s

From the numerical model, the velocities along x, y, z-directions (Velocity-u, v, w) are calculated for the magnitude of load 1 in combination with the load directions of vertical and lateral, which are plotted against time at the POI $[0, 20]$ in [Fig.5.7] . The first row consists the velocities along x, y, z when a vertical load moves and the second row considers the same when a lateral load moves.

In [Fig.5.8], the velocities generated at the POI for the load combination 2 is represented for the case of vertical and lateral direction load.

The points to observe are:

- For the case of lateral loading, velocity along v rises as the load nears the origin and reduces as it moves away, and a similar envelope of the vibrations is noticed in w for lateral loading. This is due to the fact that points along y-axis have significant velocities when the load is directly along the axis. The reverse is noticed for velocities along u due to symmetry.
- It is noticed that for the load magnitude combination of Load 2, a rise in velocity is noticed at w, v due to the vibrations caused by the spike in load at the origin. This is not noticed in u because the load at origin does not cause a velocity along u for points along $y-$axis due to symmetry. This represents a defect like encounter by the wheels of the train at the track, when a sudden change in loading occurs similar to a crossing.
- In vertical and lateral loading, there is a spike when first and last wave arrives and this is because in the numerical model, the load suddenly starts at $[-10, 0]$ and ends at $[10, 0]$ like an impulse. This can be overcome by increasing the loading domain's boundary or by smoothing out the load magnitude in the increasing and the decreasing end.

To obtain the total vibration caused, a superposition of velocities for lateral and vertical loading is done and plotted in [Fig.5.9]

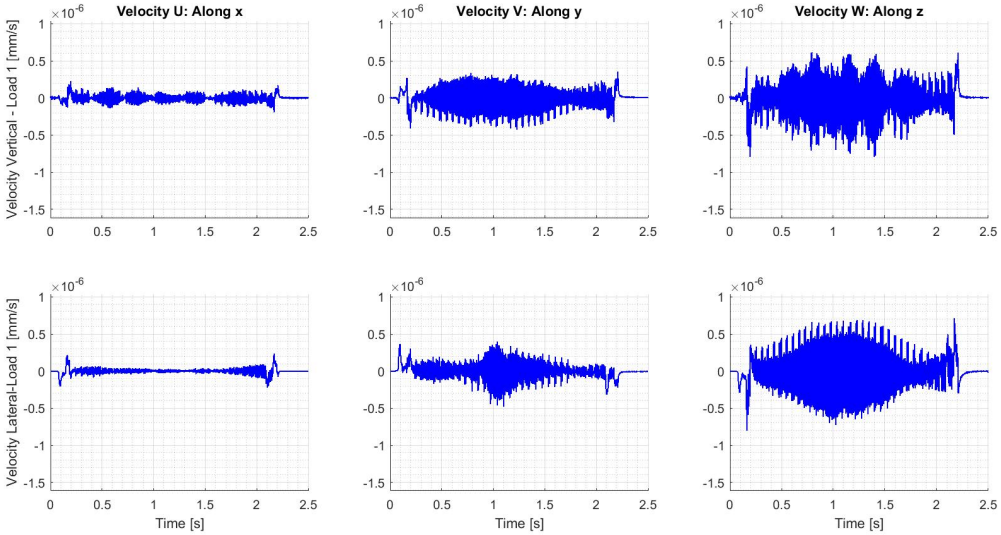

Figure 5.7: Velocities at [0,20] for a moving vertical and lateral moving Load 1 at 10m/s

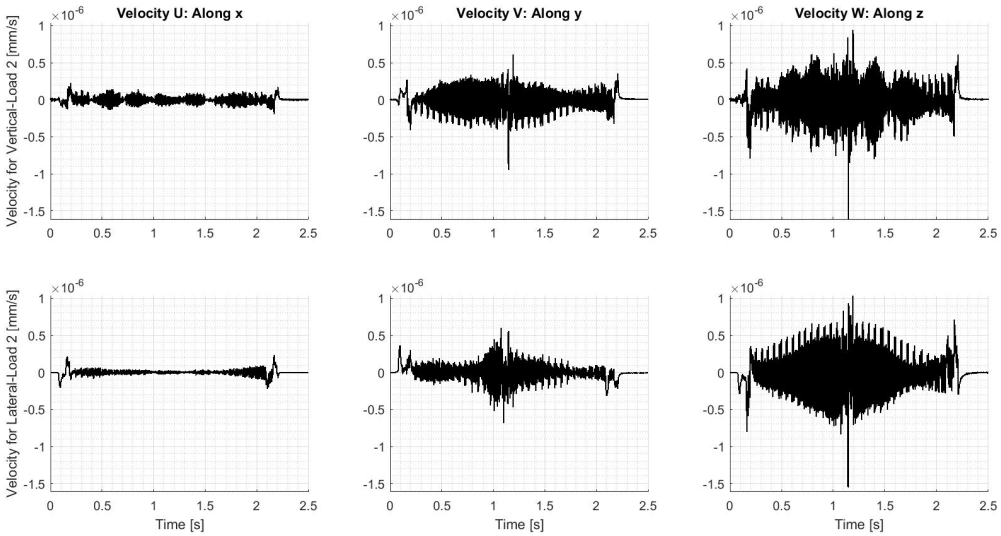

Figure 5.8: Velocities at [0,20] for a moving vertical and lateral moving Load 2 at 10m/s

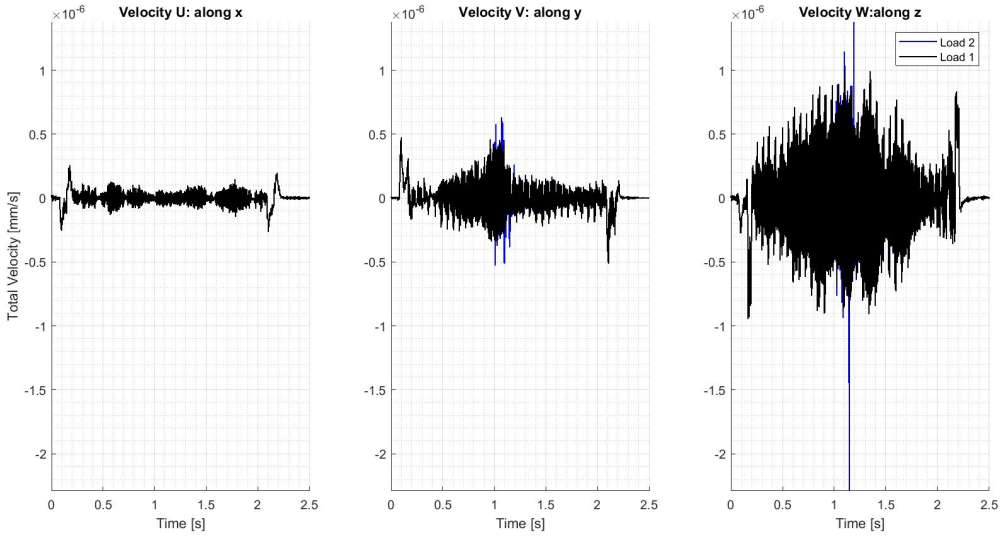

Figure 5.9: Total Velocities at [0,20] for moving load combinations of Load 1 & Load 2, moving at 10m/s

5.3.2 Multiple Speeds

For a load magnitude combination of Load 1, for when the direction is vertical and lateral, moving at multiple speeds of 10, 15, 20 & 25 m/s the velocities caused at POI $[0, 20]$ is plotted against time [Fig.5.10]. In row one, for the load-1 magnitude and a vertical direction moving load, the velocities along x, y, z directions are plotted. In row two, for the lateral direction of load moving is plotted. It is noticed that:

- The higher the speed of the load, smaller the time span of the vibrations at POI.
- The arrival of waves is at the same time for all the speeds, however, the departure time of waves differs between multiple speeds.
- The spike in arrival and departure of waves is due to the numerical boundary of the loading scheme and can be overcome by extending the boundary or by gradually increasing the load magnitude over the span of loading.

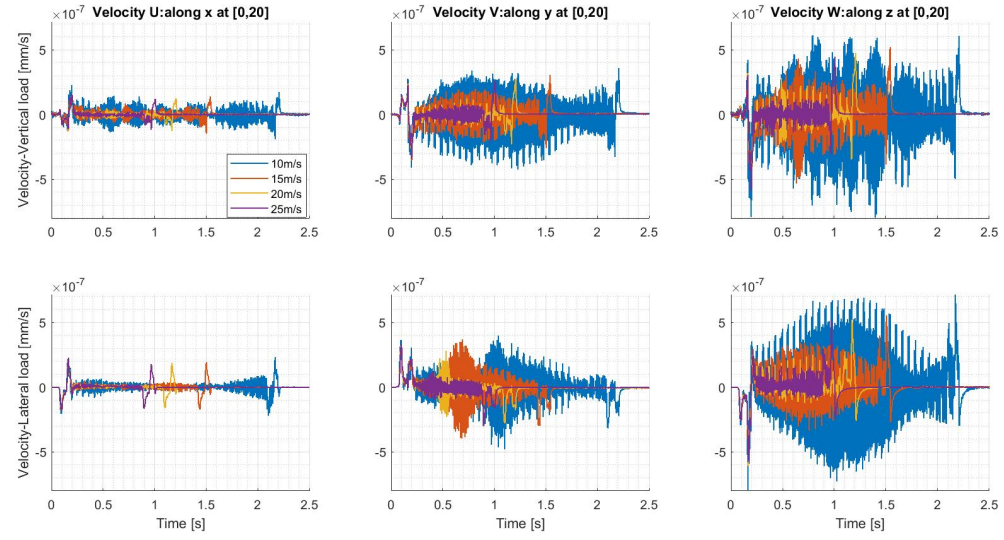

Figure 5.10: Velocities at [0,20] for moving load combinations of Load 1, moving at 10, 15, 20 & 25 m/s

The total velocity at POI is calculated as a superposition summation of velocities due to lateral and vertical load moving is in expressed in [Fig.5.11]

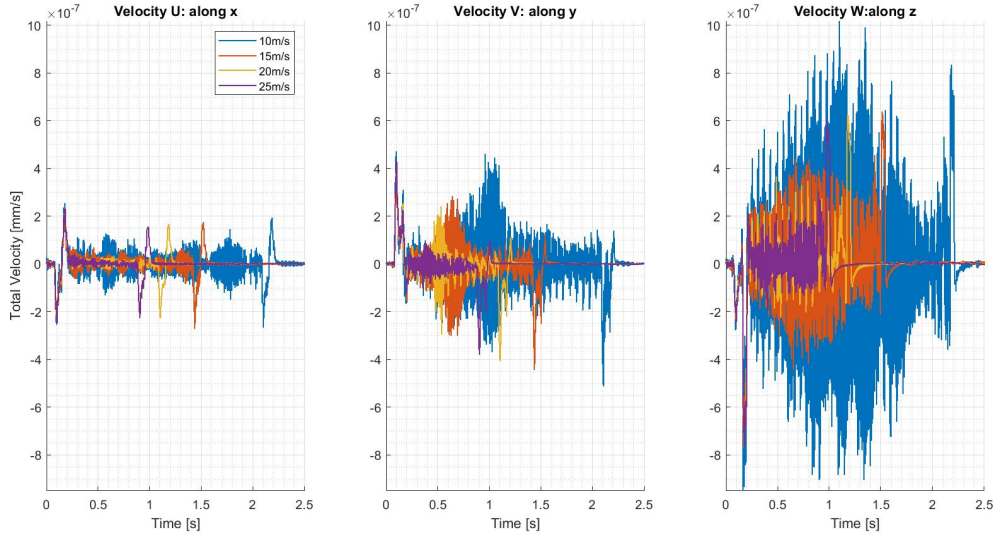

Figure 5.11: Total Velocities at [0,20] for moving load combinations of Load 1, moving at 10, 15, 20 & 25 m/s

6 MEASUREMENTS BASED COMPARISON

6.1 MEASUREMENT SETUP

6.1.1 Location

On the 9th of September 2020, near the Lochem railway station [Fig.6.1] in the Netherlands, ground vibrations generated by Blauwnet trains going through a standard turnout were measured at four points of interest. The google satellite image of the location of the standard turnout is depicted in [Fig.6.2] where a branch line path of passage is encountered by trains arriving from Oldenzaal halting at Lochem station and the main line passage is encountered by trains departing from Lochem station to Oldenzaal. The turnout consists of a single switch and a crossing 34.5 m apart where a single lane railway whose width is 2.6 m spans out to two lane railway towards the Lochem station to aid the trains to arrive and depart from two platforms available at the station. The location of interest near the railway track where the measurement sensors were placed is vegetated with wild plants which were cleared partially at the points where the sensors were placed. The soil is almost homogeneous in the top layer and has a shear wave velocity of $150 - 200$ m/s derived from CPT test as referred to via DinoLocket.

Figure 6.1: Lochem Railway track

Figure 6.2: Google Satellite image of the location

6.1.2 Sensors Setup

The SYSCOM sensors [Fig.6.3] were setup as depicted in [Fig.6.4].It measured the vertical, transversal and longitudinal velocity responses in the free field simultaneously. The three available sensors were

placed in phases of time in order to acquire measurements from four points of interests in combinations of : (A, B and C) and (A, B and D).

Figure 6.3: Sensor Setup

Point A is closer to the switch at a distance of 8.3 m and it is a point of interest as the ground vibrations from near the starting point of the turnout can be measured. Point B is near the crossing, as it is the point where there exists a discontinuity in the contact between the rails and the wheel, therefore measurements from near the crossing is of interest. Point C is perpendicularly 25 m away from point B and insights on geometrical damping can be inferred from C and B. Point D is 40 m away from the crossing, therefore it is the measurement standard for when a train passes through a railway track, ideally without any influence of the turnout components, however in this circumstance due to the length of the train being slightly higher than the distance between point B and D, the influence exists.

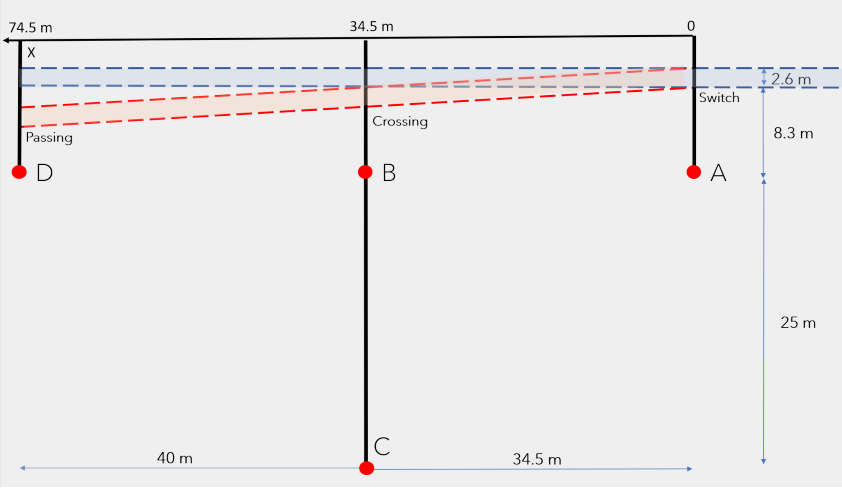

Figure 6.4: Schematic diagram of the sensors setup

6.1.3 Train

The Blauwnet trains [Fig.6.5] passes through the turnout at Lochem. With a length of 41.8 m they have an axle load of 18 tonnes with three sets of double axle bogies spaced at 16.5 m. The trains encounter the turnout at an accelerating or decelerating speed of approximately 16.5 m/s (derived from videos taken on site) when arriving or departing from Lochem station.
Four trains pass through the turnout per hour, two in each direction:

XX:10 hr, XX:40 hr : Oldenzaal → Lochem
XX:20 hr, XX:50 hr : Lochem → Oldenzaal

Figure 6.5: Train passing through the turnout

6.2 MODEL SETUP

The turnout model explained in Chapter 5 is considered to match the measurement setup. The points of interest are now points A, B, C and D. Similar to the previous model, two cases are considered: a vertical and a lateral moving load, whose result of vibrations are superimposed in the point of interest. In order to compare the numerical model to the measurements the assumptions considered are:

- Numerical model assumptions
- Points of interest
- Loading assumption

Numerical model

The numerical model assumptions are listed in Table 6.1.

Domain (Ω)	Name	Value	Unit
Half-space	Shear Modulus of half-space (μ)	5.97×10^7	N/m^2
	Poisson's Ratio (ν)	0.3	
	Material Damping	2.5%	
	Density of half-space (ρ)	1950	kg/m^3
	Longitudinal wave speed (c_l)	$327.50 + 8.18i$	m/s
	Transverse wave speed (c_t)	$175.05 + 4.37$	m/s
	Rayleigh wave speed (c_r)	$162.13 + 4.05i$	m/s
Beam	Mass of beam (m)	760	kg/m
	Flexural Rigidity (EI)	1.29×10^7	Nm^2
	Width of beam (2a)	2.6	m

Table 6.1: Numerical Model Details

Points of Interest

The points of interests are A, B, C and D. Their coordinates with respect to y-direction is derived from [Fig.6.4]. The coordinates along x-direction is always zero, as the model's origin changes with respect to the point of interest.

Load assumption

The train is considered as a moving point load (vertical and lateral), as described in Chapter 5. However, it has three sets of double axle wheel sets, each of which is considered as a moving load. Thus, there are three moving loads as detailed in [Eq.6.1]:

$$F_b(x,t) = \sum_{j=0}^{N-1} P(x)\delta(x - v(t + T_j)) \tag{6.1}$$

Where N is the number of wheel-sets (3), $P(x)$ is the load magnitude which changes with respect to position and v is the velocity of the train. T_j is the lag in time for the wheel-set j with reference to the first wheel-set as expressed in [Eq.6.2]:

$$T_j = j\frac{L_w}{/}v \tag{6.2}$$

L_w is the length of the carriage, i.e the spacing between the wheel-sets.
Numerically, an assumption of three wheel-sets is assumed which are spaced at 16.5 m away from each other moving at 16.5 m/s and the magnitude of the load with respect to space is expressed in [Fig.6.6]. The figure considers the origin as the switch, whereas when the load is applied on the model, the values of magnitude is viewed with respect to the new origin which is relative to the point of interest. For example, if the POI is $(35, 9.6)$, then the value of the graph $(P(x))$ is transformed to $(P(x - 35))$.

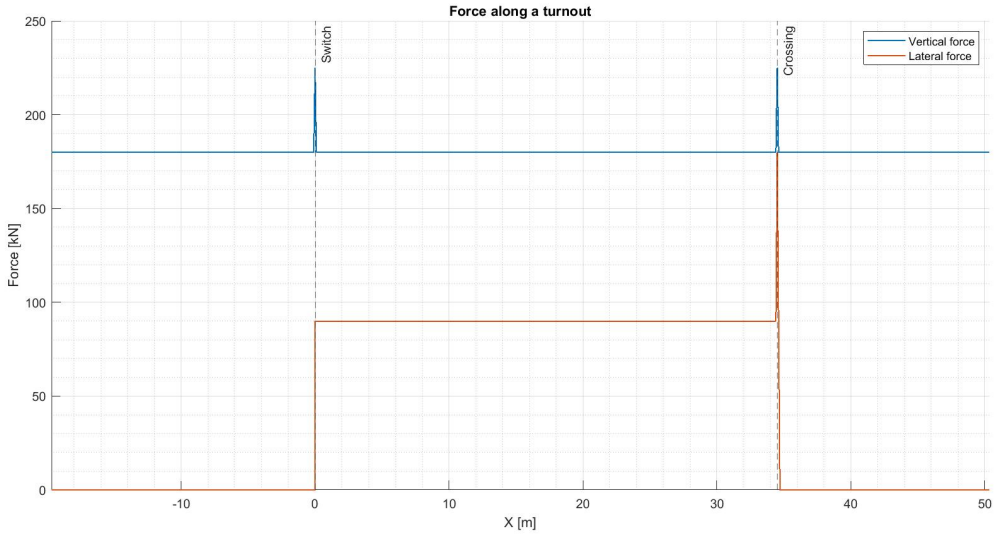

Figure 6.6: Force across the turnout

The lateral forces exist only in the section of the turnout with a spike noticed at the crossing, and vertical load which is equivalent to the axle load (18 t) is a constant moving load except at the switch and the crossing where a singular impact like loading occurs. This assumption is in consideration of the Literature study in Chapter 2.

6.3 COMPARISON OF MODEL AND MEASUREMENTS

6.3.1 Measurement: Turnout

A Blauwnet train that arrived at Lochem station at 15:40 hrs crossed through the turnout taking the branch line, whose ground vibrations at A, B and C are recorded along x, y and z directions are expressed in [Fig.6.7].

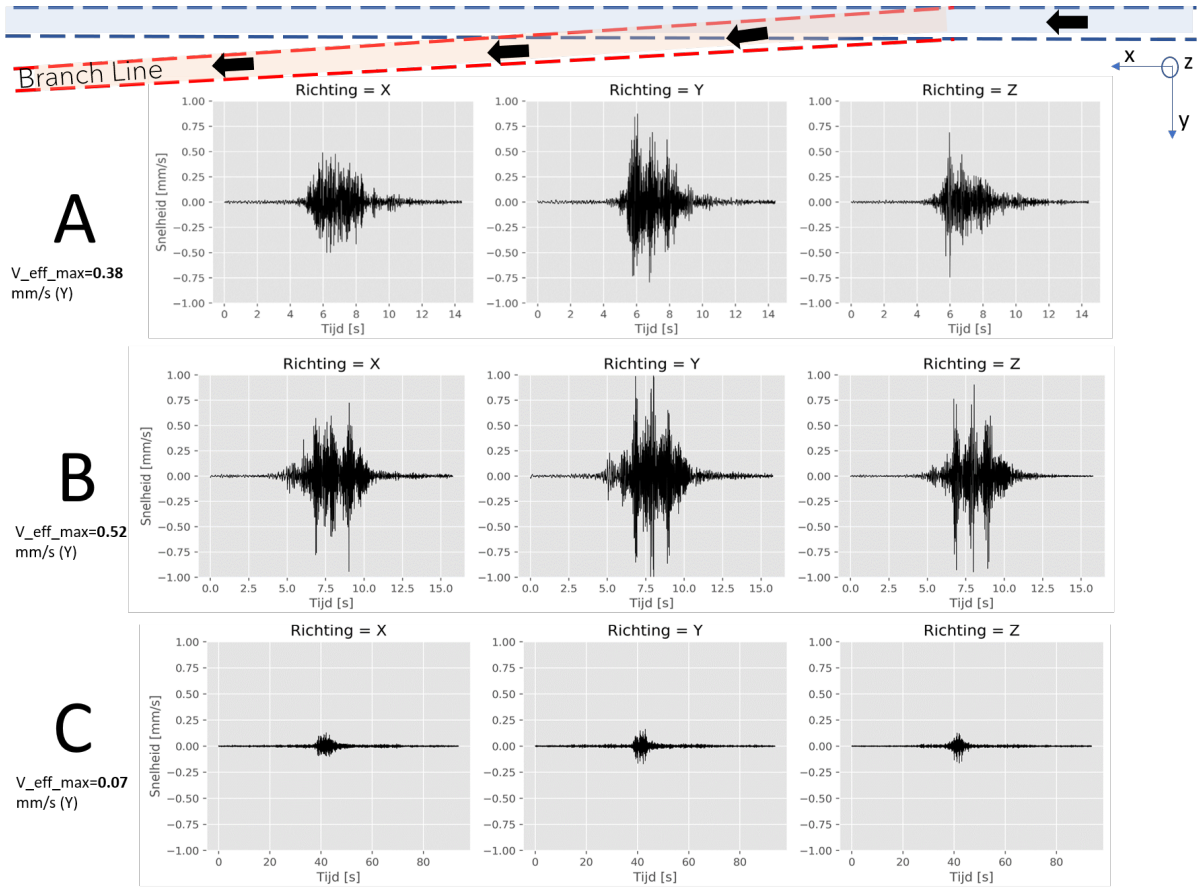

Figure 6.7: Measurements analysed at sensors A, B and C for a train moving along the branch line

With the effective maximum velocity $v_{eff,max}$ calculated as per SBR-B Guideline, as explained in Chapter 2. The following are the points of observation from the measurements in [Fig.6.7] :

- **A**: The $v_{eff,max}$ is 0.38 mm/s along y-direction with time span of the vibration being almost 6 seconds. There exists three sharp peaks in the vibrations co-relating to the three wheel-sets. The tail in the vibration can be attributed to the vibrations received from the passing of the train towards the crossing. The first wheel-set causes higher vibration than the trailing wheel-sets. The three peaks are distinctly visible along y and z and not along x.
- **B**: The $v_{eff,max}$ is 0.52 mm/s which is the maximum of measured velocities by the sensors, therefore it can be observed that the crossing causes the maximum vibration in correspondence to the literature study in Chapter 2. The three sharp peaks in the measurements relates to singular impact like loading by the wheel-sets when it encounters the crossing.
- **C**: The $v_{eff,max}$ is 0.07 mm/s where the vibrations have damped almost 86.5% from point B within a distance of 25 m. The singular impact is not as prominent as at point B. However the time span of vibration is larger in comparison to A,B as point C is farther away, therefore for all the source induced ground response to reach C takes larger time span.

Standard railway

When the train passes through the railway track away from the influence of the turnout zone, the vibrations are recorded at point D. For a train that passed through at 19:40 hrs the vibrations were recorded at points A, B and D which are points close to the switch, crossing and a normal railway track respectively and depicted in [Fig.6.8].

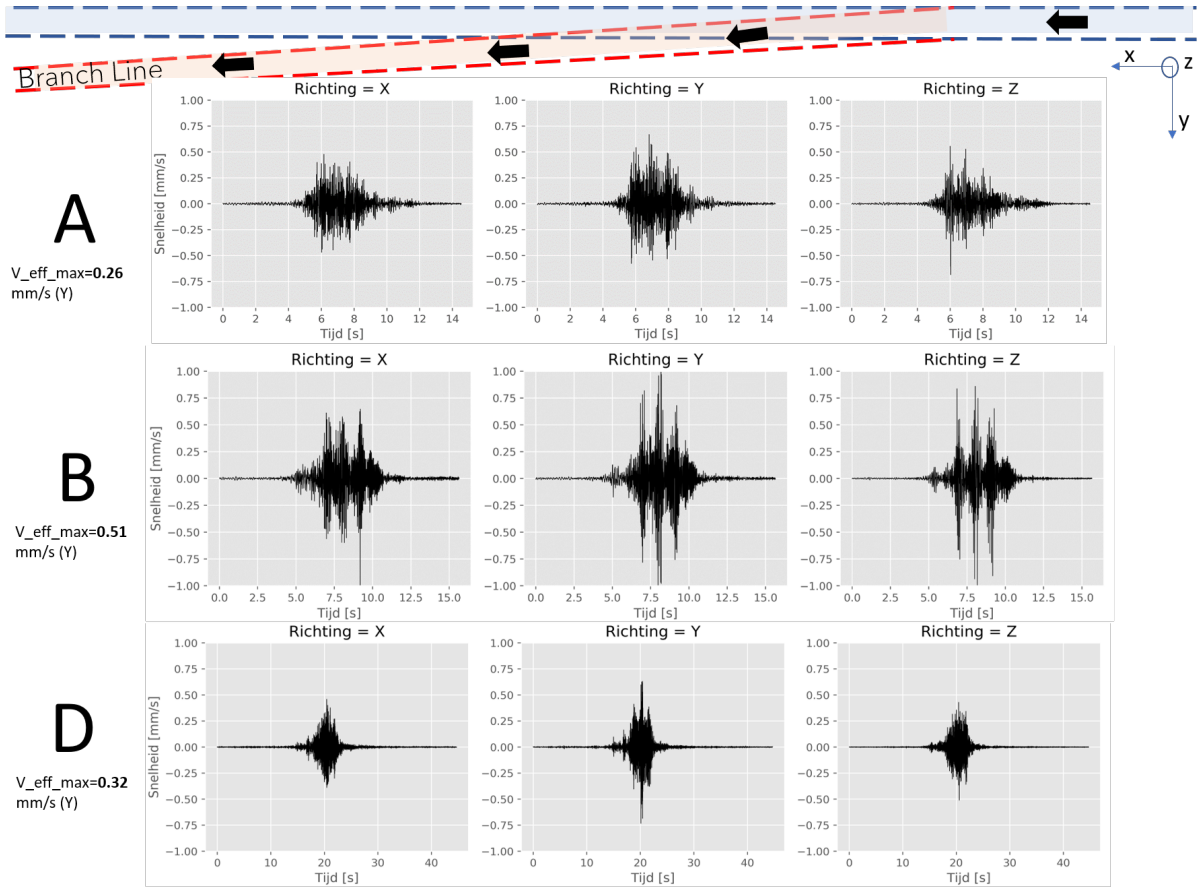

Figure 6.8: Measurements analysed at sensors A, B and D for a train moving along the branch line

The notable observations from the measurements at D are:

- **A**: The $v_{eff,max}$ is 0.26 mm/s, similar to [Fig.6.7] there exists three distinct peaks caused due to three wheelsets along with a tail of vibration. The response along x, y and z are of similar range in magnitude with the peaks being distinct along y and z.
- **B**: The $v_{eff,max}$ is 0.51 mm/s, similar to [Fig.6.7]. The response along B is the maximum, confirming that the response near the crossing is of maximum disturbance. The arrival of P waves is clearly visible at around 5 seconds. The response along y is the highest followed by z.
- **D**: The $v_{eff,max}$ is 0.32 mm/s which is lower than point B which is close to the crossing, but higher than point A [Point D is closer to the railway track than point A]. It is also noted that the three sharp peaks as observable in point A and B is not noted in D therefore confirming that impact like loading does not occur for a simple passing of the train like it occurs in a crossing or a switch. The train is also decelerating when it nears the station, thus the speed of the train is lower at point D.

6.3.2 Model:Turnout

On co-relating the model to the best to match the measurement setup, the results obtained for vibrations obtained at A, B, C and D based on the model are depicted in [Fig.6.9].

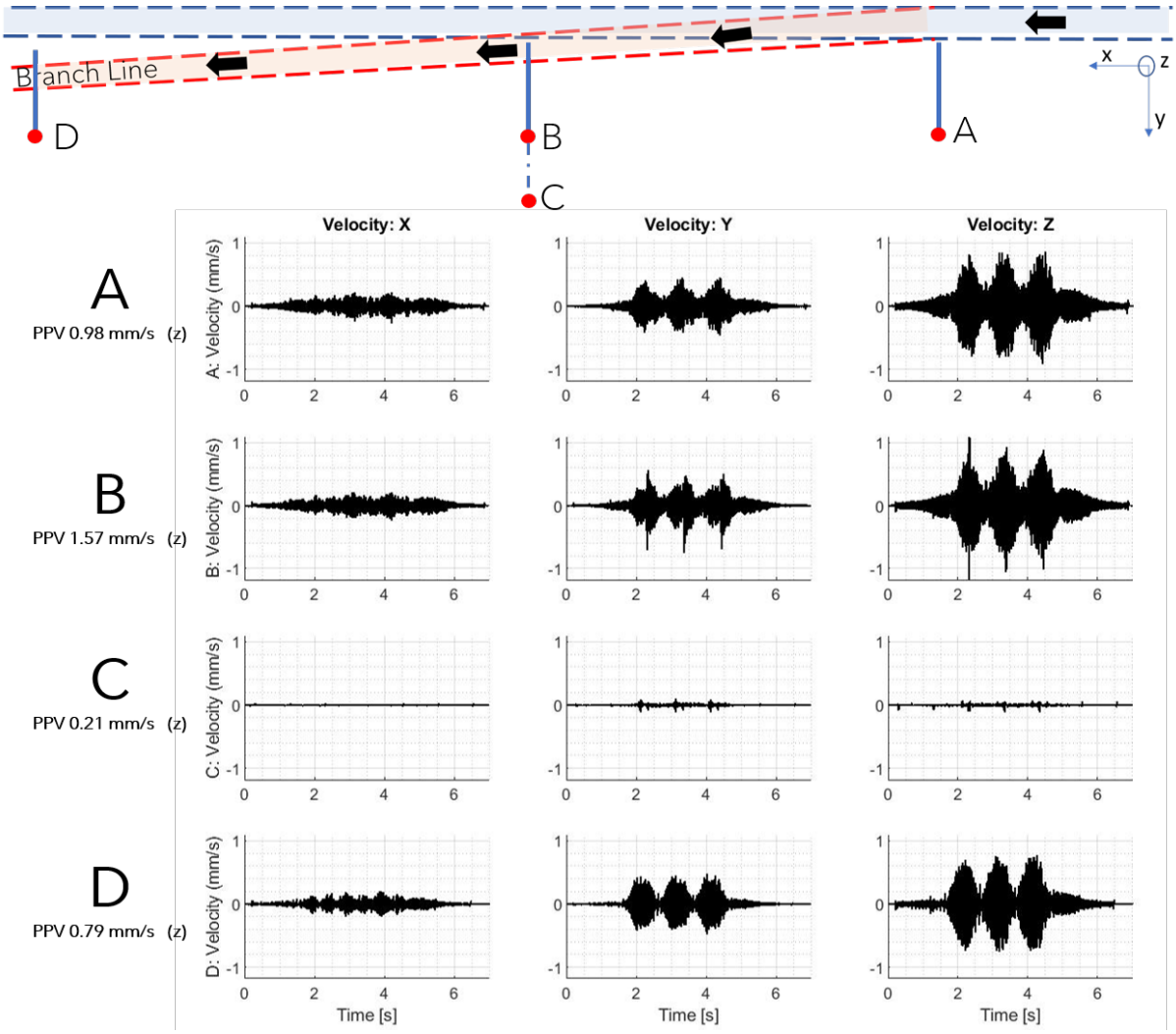

Figure 6.9: Ground velocity derived from model for a train moving along branch line at 16.5 m/s

The points to observe from the model based results are:

- **A**:The peak particle velocity (PPV) is 0.98 mm/s with three distinct envelopes in the ground vibrations. This is related to the three wheel-sets. The time span of vibration is almost 6 seconds, which relates to the speed of the load. The three envelopes of vibrations that increase initially and then decrease,corresponds to the wheel coming closer to the point and moving away respectively. Apart from the envelope, three steeper spikes are visible on top of the envelope, which is due to the sudden increase in lateral loading at the start of the turnout.
- **B**:The peak particle velocity (PPV) is 1.567 mm/s with three distinct envelopes in the ground vibrations. The peaks are higher than in point A, as it is near the crossing with higher impact loading. The steeper peak on top of the envelope is the cause of PPV as the load at the crossing is higher vertically as well as laterally.
- **C**:With point C being farther away, the PPV is 0.208 mm/s. This is 86.7 % reduction in PPV over a distance of 25 m.
- **D**: The PPV is 0.795 mm/s which is 19.3 % decrease when compared to point A and 49.26 % decrease when compared to point B. Although the distance from the beam is the same, the drop in magnitude occurs due to the loading scheme. There exists no lateral loading near point D, however vertical axle loading is present and that is the source of difference between D and B & A. This scenario correlates to the normal moving of a train, therefore the envelopes of vibrations are more smoother in nature than the spike-y vibrations noticed in A and B.

The overall shape of the loading is similar over point A, B and D as they are at the same distance from the beam and point C is farther away but the type of wave (three-peaks visible nature) is similar. Although, the magnitude of the PPV is the source of difference between the points. Vibrations along z-direction is the highest for all.

Discussion on Comparison

The model based ground response is compared qualitatively and quantitatively to measurements obtained and the similarities and differences between them are drawn up to discuss the performance of the model.
The similarity between the measurements and the model is visible in the envelope of the ground vibrations vs time, along with the time span of the result. The difference between the measurement and model is primarily seen in the direction of vibration and the magnitude of it. In the following section the attribute and cause of similarity and differences between the measurements and the model are discussed.

Differences

The following are the attributes of difference between the model and measurement scenario and the possible causes of the choices made:

1. **Loading spectrum** : The vehicle dynamics is crucial in a turnout scenario due to the accuracy required in the loading spectrum. The magnitude of the load, which leads to the derivation of PPV at a point on surface can be calculated with accuracy if the force spectrum is accurate. In the model above, a simple loading model is chosen from literature study.Alfi and Bruni [2009]

2. **Deceleration and acceleration**: The changing speed of the train is not considered, as these cause drag forces in the rails which in turn causes longitudinal loading. Only two types of loading: vertical and lateral are considered in the model which are then super-imposed to obtain the result. Therefore, on inclusion of longitudinal loading complex cases of varying speed can be fit into the model.

3. **Bending stiffness of beam**: In the model, the bending stiffness of the beam is assumed the same for vertical loading and lateral loading. Although vertically this is almost accurate, laterally this is bound to be different. The presence of ballast and sleepers affect the bending stiffness of the system in the lateral direction which is not accounted for. The effect of the beam is visible for a distance of almost 25 m for the model (Chapter3), therefore for points of interest within this radii, the bending stiffness accuracy will be important.

4. **Railway components**: The presence of sleepers, ballast affect the magnitude of the force being transferred to the soil. Although the interaction is smeared over the width of the structure, the magnitude of this force is a playing factor in finding accurate ground vibration.

5. **Curvature of rails**: The curvature of rails is not considered. Although the effect of this is assumed to be captured by the lateral forces assumed in the closure panel, the beam's interface condition with the half-space surface is not complex enough to handle a curved condition.

6. **Wheel-sets**: From Burgelman and Bahn [2015] the lateral forces generated is a function of the wheel-set that negotiates the turnout, that is, each wheel set exerts a different force. This is not included in the model.

7. **Interaction Force**: The railway guiding system is assumed as a beam which exerts a constant force along the beam width (2a) in the model. However in reality, this is not the case. The complex components of the railway system, exerts a distributed force across the width of the system. This can be handled by approaching the interface condition more complexly, as explained in Steenbergen and Metrikine [2007].

8. **Change in stiffness of tracks**: Due to the presence of stock, guiding rails at the switch and a nose in the crossing , change in track stiffness is expected, along with the presence of a two way lane as a comparison of a single way lane near the switch. Change in track stiffness affects the vibration magnitude in closer range points of interest. Andersson and Dahlberg [1999]

Similarities

The model and the measurements are on a comparitive bases of similarity along the following lines:

1. **Moving load**: A moving load causes the envelope of ground vibrations to be of increasing in nature as the load nears the point with time and a decrease as the load moves away. This is on similar lines between the model and measurements with the P-waves arriving first and the surface waves arriving after back to back for the three-wheelsets. This confirms the logical working check of the model.

2. **Time span of vibration**: With almost equal (6 seconds) of time span of the vibration from the model and measurement, the speed of the train in reality and the moving load in the model, is almost equal. Therefore, the effect of change in speed between the switch and the crossing is negligible.

3. **Double loading model**: The concept of having two models, one with a moving vertical load and another with a moving lateral load, has aided in more accurate modelling of the turnout scenario, as the total displacement is the superposition of the two. This leads

4. **Points of interest**: Although this is a self-made choice, it is a crucial factor in analysing the consequences of a turnout. Points near a crossing are more impacting in analysing this from the effective velocities of the measurements and the PPV of the model. Therefore, point B experiences higher ground vibrations as it is near the crossing.

7 CONCLUSION, RECOMMENDATIONS & DISCUSSION

7.1 CONCLUSIONS

The conclusions are approached in three phases:(a) The modelling method ;(b) Comparison with measurements and (c)Addressing the research objective

7.1.1 Modelling method

The objective of the thesis is to qualitatively and quantitatively be able to describe the ground vibrations caused due to a railway turnout. To achieve so, a semi-analytical impulse model was approached in Chapter 3 and 2. Based on the impulse model, a moving load spectrum model was built based on it, to depict a turnout like system. The following are the conclusions drawn from the modelling approach:

a. Impulse Model

Qualitatively:

- Qualitatively, the superposition of two models: the vertical and lateral direction of loading a semi-analytical model, achieves the result of producing sound results in ground response checked through the arrival of waves.
- The interaction force which is the primary source of excitation on the soil from the beam dampens quickly for the case of lateral impulse when compared to vertical impulse, for the given numerical model.
- The model and procedure approached can be used to find vibrations at any depth and not just at the surface. This is so because, the solution at $z = 0$, is the final step to the process.

Quantitatively:

- For the case of lateral model, the equivalent stiffness of the soil provided to the beam is a function of the bending stiffness and the behaviour of the beam. Therefore, detailed modelling of it, through inclusion of sleepers and ballast is necessary in achieving quantitatively accurate ground response.
- On numerically approaching the solution of ground displacements, the truncating limit of the frequency domain while Fourier transforming it to time domain has led to disturbances existing at $t = 0$ and this can be tackled by using a low pass filter, or applying an applicable load.

b.Moving Load Model

Post building the impulse model, a moving load is achieved as a convolution of the impulse responses. On doing so, the following are the conclusions:

Qualitatively:

- Qualitatively the moving load model can be used to visualise and analyse a single-bogie moving induced response on the ground achieved through convolution of the responses from a series of impulses. Therefore, the step size of the loading domain along the beam is important in the accuracy of the result (and also expensive).
- In the moving load model, the model of vertical and lateral load is solved individually and superimposed. Therefore, the beam behaves independently to both the loading and the response, and thus the responses are not interlinked.

- With the current model, any defect like scenario (vertically and laterally) in the tracks can be modelled along with correct load spectrum to obtain the ground response.

Quantitatively:

- The numerical boundary of the loading domain plays a role in the accuracy of the response in the arrival and departure of waves. This can be improved by increasing the domain of loading, or by smoothing out the loading and unloading process. Increasing the loading domain would be computationally heavy.
- The response along z-direction is the highest for the case of lateral or vertical loading. This is because z-direction response is highest for surface waves.
- For the case of lateral loading, although y-direction response is expected to be highest, it is not so because: during the arrival of P-wave there is a strong y-component when a lateral load is applied, however the surface waves which are higher in magnitude bring in higher z component.
- Quantitatively, the presence of the beam is essential in modelling a moving load when the point of interest is in a close range of 25-30 m for the given numerical model.
- The curvature of the beam can be neglected as radius of curvature of tracks are sufficiently large to assume an infinitely long Euler Bernoulli beam.

7.1.2 Comparison with measurements

The model is compared against measurements obtained in Chapter 6. Detailed conclusions has been discussed in the previous chapter on the differences and similarity between the model and measurements, however the following are the vital conclusions derived:

- **Measurements**: To observe a turnout's impact the crucial points are near the crossing and the switch and the sensor points were placed accordingly. From the measurements, the crossing is the source of maximum ground vibration. Also, since it was a simple train that passed through a standard turnout, the ground vibrations were more visibly logical to understand.
- **Model**: The model used to validate the measurement has been altered to match the magnitude of the properties of soil. Qualitatively, the model behaves similarly to the turnout system in the case of crossing and switch. However, quantitatively, the current assumptions are insufficient. A detailed vehicle-dynamics induced load spectrum along with field study of the interaction force is necessary.
- From the measurement and the model, a crossing behaves like a singular impact. Therefore, if only PPV is considered then a singular loading is sufficient to analyse the ground vibrations.

7.1.3 Research Objective

Qualitatively and Quantitatively, what are the ground vibrations at points of interest when a train negotiates a railway turnout?

The current model approaches a turnout as a loading scheme in the vertical and lateral direction on a semi analytical system. By doing so, qualitatively, from literature study and from measurements it is able to achieve the phenomena behind a turnout, that is impulse like loading at crossings in both the directions. The response near a railway turnout can therefore be described by a dual load model. However, to achieve quantitative accuracy, the lateral model has to be upgraded to handle complex track geometry of ballast and sleepers in order to achieve accurate equivalent stiffness provided by the soil. This can also be achieved through field study of the interaction force.

7.2 RECOMMENDATIONS

The recommendations are made, keeping in mind the goal of understanding the ground vibration caused by a railway turnout. Therefore:

- **Model** : A detailed sleeper-ballast model can be used instead of a single euler bernoulli beam.
- **Load spectrum** : A measurement based load spectrum can be used by obtaining the impact loading on wheels in a crossing.
- **Response**: Apart from ground response $z = 0$, at any depth z, the vibrations can be derived from the model.
- **Analysis**: The effect of speed and other railway defects can also be analysed with the current model.
- **Measurements**: Further measurements from near track response to analyse interaction force will be useful to update the model. The measurements from impact of rail-wheel would also lead to accurate load spectrum input.

7.3 DISCUSSION

The modelling choices made is analytical which is essential in understanding the vertical and lateral load that occur in the problem. By approaching it as two independent problems has and super imposing the response has led to a easier compartmentalisation of the results to view each load's response.

Apart from separating the loading factor, separating the domains also helps in simplifying the problem. Therefore now there is a domain for load input on beam and another for load input on the soil. By doing so, at any point if the complexity is not sufficient, then the loading spectrum can be obtained from measurements or other methods and then input-ed into the model for the final ground vibration result. The method of finding an interaction force which is a function of frequency and wavenumber, leads to a more complex and realistic way of approaching the force distribution. This not only helps in ground vibration problem, but can also be used for analysing the beam's behaviour. Therefore, for a crossing or switch's maintenance and repair apart from impact loading from the vehicle, resistance from the soil also exists which is calculated from the interaction force.

The physical system's numerical values can be improved in many ways as described in above sections, from including a complex track geometry to back tracing to an accurate load spectrum. Numerically, the model can be improved by expanding the domain of integration. Conceptually, curvature of tracks can be neglected along with longitudinal induced vibrations. This is derived so from the measurements.

Lastly, the given model is step two solution of a bigger problem. Step one can be anything from a turnout or a railway defect to any dynamic load moving. This is so because, the load input has to be fit into the model and the resultant ground vibration can be calculated from it. The model can also be used to calculate vibration at a different depth by substituting the appropriate depth in the final step of the solution.

BIBLIOGRAPHY

Aki, K. and G.Richards, P. (2002). *Quantitative Seismology*. University Science Books, Sausalito, California, second edition.

Alfi, S. and Bruni, S. (2009). Mathematical modelling of train-turnout interaction. *Vehicle System Dynamics*, 47(5):551–574.

Andersson, C. and Dahlberg, T. (1999). Load impacts at railway turnout crossing. *Vehicle System Dynamics*, 33(SUPPL.):131–142.

Burgelman, N. and Bahn, D. (2015). Some Preliminary Results in Simulation of Interaction between a Pushed Train and a Turnout SOME PRELIMINARY RESULTS IN SIMULATION OF. (August 2011).

Connolly, D. P., Galvín, P., Olivier, B., Romero, A., and Kouroussis, G. (2019). A 2.5D time-frequency domain model for railway induced soil-building vibration due to railway defects. *Soil Dynamics and Earthquake Engineering*.

Connolly, D. P., Marecki, G. P., Kouroussis, G., Thalassinakis, I., and Woodward, P. K. (2016). The growth of railway ground vibration problems — A review. *Science of the Total Environment*.

Dieterman, H. A. and Metrikine, A. (1996). Equivalent stiffness of a half-space interacting with a beam. Critical velocities of a moving load along the beam. *European Journal of Mechanics, A/Solids*, 15(1):67–90.

J. D. ACHENBACH (2003). *RECIPROCITY IN ELASTODYNAMICS*.

Kouroussis, G., Connolly, D. P., and Alexandrou, G. (2015a). Railway ground vibrations induced by wheel and rail singular defects. 3114.

Kouroussis, G., Connolly, D. P., Alexandrou, G., and Vogiatzis, K. (2015b). The effect of railway local irregularities on ground vibration. *Transportation Research Part D: Transport and Environment*.

Lamb, H. (1904). On the propagation of tremors over the surface of an elastic solid. *Philosophical Transactions of the Royal Society of London. Series A, Containing Papers of a Mathematical or Physical Character*, 203:1–42.

Liu, X. and Markine, V. L. (2020). Train hunting related fast degradation of a railway crossing-condition monitoring and numerical verification. *Sensors (Switzerland)*, 20(8).

Pletz, M., Daves, W., and Ossberger, H. (2012). A wheel set/crossing model regarding impact, sliding and deformation-Explicit finite element approach. *Wear*, 294-295:446–456.

Sheng, X. (1999). Ground vibration generated by a load moving along a railway track. 228:129–156.

Steenbergen, M. J. and Metrikine, A. V. (2007). The effect of the interface conditions on the dynamic response of a beam on a half-space to a moving load. *European Journal of Mechanics, A/Solids*, 26(1):33–54.

Torstensson, P. T., Squicciarini, G., Krüger, M., Pålsson, B. A., Nielsen, J. C., and Thompson, D. J. (2019). Wheel–rail impact loads and noise generated at railway crossings – Influence of vehicle speed and crossing dip angle. *Journal of Sound and Vibration*.

Xin, L., Markine, V. L., and Shevtsov, I. Y. (2016). Analysis approach of turnout crossing performance by field measurements and finite element modeling. *The Dynamics of Vehicles on Roads and Tracks - Proceedings of the 24th Symposium of the International Association for Vehicle System Dynamics, IAVSD 2015*, pages 1593–1600.